AD-A169 136 SENSITIVITY TESTS OF A SURFACE-LAYER WINDFLOW MODEL TO EFFECTS OF STABILITY AND VEGETATION(U) AIR FORCE GEOPHYSICS LAB HANSCOM AFB MA J M LANICCI 25 OCT 85 1/1

UNCLASSIFIED AFGL-TR-85-0265 F/G 4/2 NL

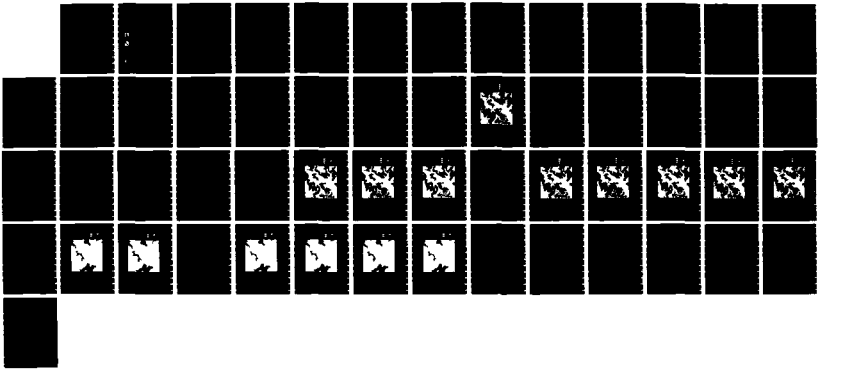

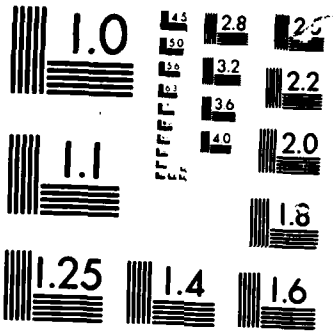

(12)

AFGL-TR-85-0265
ENVIRONMENTAL RESEARCH PAPERS, NO. 934

Sensitivity Tests of a Surface-Layer Windflow Model to Effects of Stability and Vegetation

JOHN M. LANICCI, Capt, USAF

25 October 1985

"Original contains color plates: All DTIC reproductions will be in black and white"

ATMOSPHERIC SCIENCES DIVISION PROJECT 6670
AIR FORCE GEOPHYSICS LABORATORY
HANSCOM AFB, MA 01731

This report has been reviewed by the ESD Public Affairs Office (PA) and is releasable to the National Technical Information Service (NTIS).

"This technical report has been reviewed and is approved for publication"

FOR THE COMMANDER

DONALD D. GRANTHAM
Chief, Atmospheric Structure Branch

ROBERT A. McCLATCHEY
Director, Atmospheric Sciences Division

Qualified requestors may obtain additional copies from the Defense Technical Information Center. All others should apply to the National Technical Information Service.

If your address has changed, or if you wish to be removed from the mailing list, or if the addressee is no longer employed by your organization, please notify AFGL/DAA, Hanscom AFB, MA 01731. This will assist us in maintaining a current mailing list.

Do not return copies of this report unless contractual obligations or notices on a specific document requires that it be returned.

Unclassified

SECURITY CLASSIFICATION OF THIS PAGE

REPORT DOCUMENTATION PAGE

1a REPORT SECURITY CLASSIFICATION Unclassified	1b RESTRICTIVE MARKINGS
2a SECURITY CLASSIFICATION AUTHORITY	3 DISTRIBUTION/AVAILABILITY OF REPORT Approved for public release; distribution unlimited
2b DECLASSIFICATION/DOWNGRADING SCHEDULE	
4 PERFORMING ORGANIZATION REPORT NUMBER(S) AFGL-TR-85-0265 ERP No. 934	5 MONITORING ORGANIZATION REPORT NUMBER(S)
6a NAME OF PERFORMING ORGANIZATION Air Force Geophysics Laboratory 6b OFFICE SYMBOL (If applicable) LYA	7a NAME OF MONITORING ORGANIZATION
6c ADDRESS (City, State and ZIP Code) Hanscom AFB Massachusetts 01731-5000	7b ADDRESS (City, State and ZIP Code)
8a NAME OF FUNDING/SPONSORING ORGANIZATION 8b OFFICE SYMBOL (If applicable)	9 PROCUREMENT INSTRUMENT IDENTIFICATION NUMBER
8c ADDRESS (City, State and ZIP Code)	10 SOURCE OF FUNDING NOS PROGRAM ELEMENT NO: 62102F; PROJECT NO: 6670; TASK NO: 14; WORK UNIT NO: 06
11 TITLE (Include Security Classification) (U) Sensitivity Tests of a Surface- (cont.)	
12 PERSONAL AUTHOR(S) Lanicci, John M., Capt., USAF	
13a TYPE OF REPORT Scientific Interim 13b TIME COVERED FROM _____ TO _____	14 DATE OF REPORT (Yr., Mo., Day) 1985 October 25 15 PAGE COUNT 56
16 SUPPLEMENTARY NOTATION	

17 COSATI CODES			18 SUBJECT TERMS (Continue on reverse if necessary and identify by block number)
FIELD	GROUP	SUB GR	
0401			ASL windflow model; Gauss's Principle of Least Constraints; Windflow over complex terrain; Cold air drainage

19 ABSTRACT (Continue on reverse if necessary and identify by block number)

This study examines the sensitivity of surface-layer windflow over gently rolling terrain to different stability conditions, both with and without the effects of vegetation used to modify terrain heights and determine surface roughness. The numerical model used is a version of the two-dimensional diagnostic surface-layer windflow model developed for the U.S. Army Atmospheric Sciences Laboratory (ASL) at White Sands, New Mexico. The model produces simulations of surface-layer windflow by using Gauss's Principle of Least Constraints to allow an initially uniform windfield to adjust to topography and buoyancy forces while conserving mass.

The model experiments used simulated meteorological data (at only one observation point) and detailed terrain and vegetation data (on a 51-by-51 grid with 100 m spacing) for an area covering 5 by 5 km over the Fort Polk Military Reservation in Louisiana. Results show that the model simulates topographically induced flows such as cold air drainage and upslope flow, despite the simple physics employed. We also show that the pres- (cont.)

20 DISTRIBUTION/AVAILABILITY OF ABSTRACT UNCLASSIFIED/UNLIMITED ☐ SAME AS RPT ☒ DTIC USERS ☐	21 ABSTRACT SECURITY CLASSIFICATION Unclassified
22a NAME OF RESPONSIBLE INDIVIDUAL Capt. John M. Lanicci	22b TELEPHONE NUMBER (Include Area Code) (617) 861-2971 22c OFFICE SYMBOL LYA

DD FORM 1473, 83 APR EDITION OF 1 JAN 73 IS OBSOLETE

Unclassified

SECURITY CLASSIFICATION OF THIS PAGE

Block 11 (cont.)

Layer Windflow Model to Effects of Stability and Vegetation

Block 19 (cont.)

ence of tall vegetation over the area (mainly coniferous and deciduous trees) alters the flow patterns under various stability conditions. These effects are shown to be caused primarily by changes in the terrain slopes and complexity from the nonhomogeneous vegetation. These results have important implications in the area of chemical transport and diffusion, because they mean that even gently rolling terrain influences the surface windflow, and that tall vegetation has a considerable influence as well.

Preface

The author would like to thank Mrs. Joan Ward for her sincere and dedicated assistance in the transition of the windflow model code from the ASL UNIVAC system to the AFGL computer system (both CDC and VAX machines). Her many hours of work on this project were invaluable, and this report would not have been possible without her. Additionally, I am grateful to the following people for their assistance on this project: Mr. Bruce Kunkel and Dr. Robert Banta of AFGL, Mr. Ronald Cionco of ASL, and Mr. John Byers of the Physical Science Laboratory at New Mexico State University. The climate data for Fort Polk and Lake Charles were supplied to us by the Air Force Environmental Technical Applications Center (USAFETAC) at Scott AFB, Ill. Mrs. Helen Connell did a superb job typing this manuscript.

Contents

Illustrations

Illustrations

Tables

Sensitivity Tests of a Surface-Layer Windflow Model to Effects of Stability and Vegetation

1. INTRODUCTION

In early 1984, we undertook an effort at AFGL to acquire an appropriate two-dimensional windflow model for use in conjunction with a Gaussian puff diffusion model developed by Fleischer[1] and evaluated and modified by Kunkel.[2,3] It is our intent that this combined prediction system for toxic chemical transport and diffusion be adapted for use by the Air Weather Service (AWS) over regions of complex terrain.

We conducted the search for an appropriate windflow model with the following constraints in mind:

(1) The model must be applied over complex terrain.

(Received for publication 16 October 1985)

1. Fleischer, M.T. (1980) SPILLS - An Evaporation/Air Dispersion Model for Chemical Spills on Land, Shell Development Company, Westhollow Research Center, Houston, Tex.
2. Kunkel, B.A. (1983) Comparison of Evaporative Source Strength Models for Toxic Chemical Spills, AFGL-TR-83-0307, AD A139431.
3. Kunkel, B.A. (1984) An Evaluation of the Ocean Breeze/Dry Gulch Dispersion Model, AFGL-TR-84-0313, AD A157165.

2. The model must be adaptable to either a small minicomputer or a microcomputer.

3. The model must be adaptable to run as a combined system with the AFGL dispersion model.

4. The model must be adaptable to small horizontal-grid spacings (on the order of 100-400 m) on a horizontal domain approximately 10 by 10 km or smaller.

Given these constraints, we reduced the number of models available for consideration to a list of six. A summary of the major features[4,5,6,7,10,11,12] and the disadvantages[8,9] of each model considered is given in Table 1. From the information contained in Table 1 and the prescribed requirements listed above, we selected the U.S. Army Atmospheric Sciences Laboratory (ASL) model for development and incorporation into the combined transport and diffusion prediction system.

This report summarizes the results of the first phase of the windflow model evaluation. In this report, we will discuss the modifications made to the ASL model to produce more realistic simulations of surface-layer windflow. We will then describe the sensitivity tests performed with the model using simulated meteorological data and detailed vegetation and terrain data supplied to us by ASL for Fort Polk, La. Model sensitivity was tested for different stability conditions (for

---

4. Ball, J.A., and Johnson, S.A. (1978) Physically Based High Resolution Surface Wind and Temperature Analysis for EPAMS, ASL-CR-78-0043-1, U.S. Army Atmospheric Sciences Laboratory, White Sands Missile Range, N. Mex.

5. Holdeman, J.T. (1982) Modeling the tropospheric wind field over complex terrain, Symposium on the Composition of the Non Urban Troposphere, Williamsburg, Va.

6. Dickerson, M.H. (1978) MASCON - A mass-consistent atmospheric flux model for regions with complex terrain, J. Appl. Meteorol. 17:241-253.

7. Dempsey, D.P., and Mass, C.F. (1983) A one-level mesoscale model for complex terrain, Proc. Sixth Conf. on Numerical Weather Prediction, Am. Meteorol. Soc., Boston, Mass. 343-347.

8. Haltiner, G.J. (1971) Numerical Weather Prediction, Wiley, New York.

9. Walmsley, J.L. (1983) Modeling of Boundary-Layer Wind Flow Above Complex Terrain: A Review, Report ARQB-83-005-L, Atmospheric Environment Service, Downsview, Ontario.

10. Lavoie, R.L. (1972) A mesoscale model of lake-effect storms, J. Atmos. Sci. 29:1025-1040.

11. Lavoie, R.L. (1974) A numerical model of trade wind weather on Oahu, Mon. Wea. Rev. 102:630-637.

12. Fox, D.G., Fosberg, M.A., Marlatt, W.E., and Reeser, W. (1976) Analysis of mountain air quality, Proc. Third Symposium on Atmospheric Turbulence, Diffusion, and Air Quality, Am. Meteorol. Soc., Boston, Mass. 470-475.

example, stable, unstable, neutral), effects of horizontally varying roughness, and reaction to the presence of nonhomogeneous vegetation over the domain.

2. THE WINDFLOW MODEL

In this section, we give a brief description of the ASL windflow model and describe the modifications made to it at AFGL. Details of the model are given by Ball and Johnson,[4] Ohmstede,[13] Ohmstede and Stenmark,[14] Cionco,[15] and Amlicke and Coleman.[16]

2.1 General Characteristics of the Model

The model produces a two-dimensional (x-y plane) surface-layer windflow analysis by employing Gauss's Principle of Least Constraints to adjust an initially uniform windfield to conform with topography, mass conservation, and buoyancy forces. Since an excellent discussion of Gauss's Principle of Least Constraints appears in Lanczos,[17] we just present the basic model constraint equation:

$$\int_{\text{volume}} [A - B_{11}]^2 \, dV \rightarrow \text{minimum}, \tag{1}$$

where A includes only the advection terms of the acceleration and B_{11} denotes the surface parallel component of the buoyancy [(see Eq. (7)]. This integral is taken over the volume of the model surface layer, which is divided into "flux boxes" of surface normal thickness Z_c, conforming to the warped terrain surfaces. The flux form of the advection in Eq. (1) is used, and a terrain-following coordinate system is used to include effects of terrain slopes in the calculations. The total constraint integral is expressed as a sum over all the boxes in the model layer:

---

13. Ohmstede, W.D. (1981) The parameterization of battlefield dispersion-new frontiers, Workshop on the Parameterization of Mixed-Layer Diffusion, Las Cruces, N. Mex. 279-287.

14. Ohmstede, W.D., and Stenmark, E.B. (1981) A model for characterizing transport and diffusion of air pollution in the battlefield environment, Workshop on the Parameterization of Mixed-Layer Diffusion, Las Cruces, N. Mex. 416-423.

15. Cionco, R.M. (1981) A meteorological approach to chemical defense over complex terrain with vegetation, Workshop on the Parameterization of Mixed-Layer Diffusion, Las Cruces, N. Mex. 323-328.

16. Amlicke, B.B., and Coleman, L.W. (1984) High Resolution Wind (HRW) Model, MRC/WDC-R-089, Mission Research Corporation, Alexandria, Va.

17. Lanczos, C. (1970) The Variational Principles of Mechanics (4th ed), U. of Toronto Press, Toronto, pp. 106-110.

Table 1. Description of Windflow Models Considered

Model	Description	Disadvantages
U.S. Army Atmospheric Sciences Lab (ASL)[4]	A two-dimensional surface layer model suitable to small grid spacings and complex terrain. Considers anabatic and katabatic-like flows influenced by static stability. Model is run on a UNIVAC 1108 computer.	Considers surface layer only. Extrapolation into mixed layer is not recommended.
Oak Ridge, Tenn.[5]	A two-dimensional model which employs variational analysis technique for use in conjunction with a movable fine mesh, allowing a Lagrangian solution of the advection-diffusion equation (ADE) to be calculated.	If shear or turbulence on a scale larger than the scale of the mesh but smaller than the scale of the full mesh exists, the mesh may become distorted in time, leading to numerical errors in the solution.
MASCON (Lawrence Livermore Lab[6])	A two-dimensional mass-conservation model which allows the mixed-layer depth to vary in time and space. Horizontal flux fields are realistically produced through this method. Channeling effects of topography are also simulated through use of terrain (no-flow through boundaries) and temporally varying inversion heights.	Horizontal resolutions below 500 m are not advised because of problems associated with specification of terrain (obstacle cells represent terrain). The model currently runs on a CDC 7600 and takes between 50 and 70 iterations to converge to a steady-state-solution. This means model will take a long time to run on a minicomputer in present form. Wind velocity problems exist for regions where the depth of the mixed layer is shallow because of high terrain and low inversion height.

Table 1 (cont.). Description of Windflow Models Considered

Model	Description	Disadvantages
University of Washington[7]	A two-dimensional primitive equation (PE) model which can use operational temperature and wind soundings for input data (usually at 850 mb). Model is diabatic and adaptable to run on PRIME 400, Cyber 750, and CRAY 1 computers.	Horizontal grid resolutions below 3 km are not recommended because of the breakdown of the hydrostatic approximation below $\Delta x \sim$ 3 km and $\Delta z \sim 1$ km[8,9]
Lavoie[10,11]	A two-dimensional mixed-layer model which employs variable horizontal grid spacing and parameterization of clouds and precipitation. Model takes 280s CPU time on IBM 360-67.	Model assumes a well-mixed planetary boundary layer (PBL). Hydrostatic assumption breaks down for horizontal resolutions needed in our case.
WINDS (USDA and Colorado State University[12])	An inexpensive two-dimensional model which produces reasonably accurate wind speeds and directions while incorporating effects of surface heating and topography. A mass-conservation model, it uses surface temperatures, pressures, and roughness lengths to modify potential flow and employs additions of divergence and vorticity fields to the basic flow as well.	Output only yields wind flow between 1 and 2 km above ground level (AGL), so it is impractical for use as a diagnostic model for surface wind flow.

$$R_T = \sum_{i,j} R_{ij}, \tag{2}$$

where R_T is the total domain residual as computed from Eq. (1), and R_{ij} is the individual residual at each grid point i, j. A number of relaxation sweeps are then performed in the model to compute a velocity correction proportional to the steepest descent vector in the multi-dimensional velocity space, written in Eq. (3):

$$n_{ij}^k = -(\partial R_{ij}/\partial v_{ij}^k)/[\sum_{i,j,k} (\partial R_{ij}/\partial v_{ij}^k)^2]^{1/2} \tag{3}$$

where k = 1, 2 and denotes the u, v wind components, n is the nondimensional correction factor, and v is the velocity. The velocity correction is given by the following relation:

$$\Delta v_{ij}^k = 0.03\, v_o \sqrt{N \times M}\; n_{ij}^k, \tag{4}$$

where Δv_{ij}^k is the velocity correction at i, j, v_o is the initially uniform velocity, and N, M are the grid dimensions. The relaxation sweeps and windfield adjustments are performed until the residual of the integral in Eq. (1) begins to "converge" to a minimum value.

There are several reasons why a variational approach is appropriate for this modeling application. Ball and Johnson[4] stated that the advection terms of the momentum equation are dominant at this scale, and it is obvious that thermal stratification is important in the forcing of topographic flows. Variational techniques have been used to derive the equation of motion for inviscid, incompressible flow.[4, 18] Considering the points mentioned above and the small space scale involved, it makes sense to use a variational approach to the simulation of the surface wind field over complex terrain considering advection, buoyancy*, detailed topography, and mass conservation (a consequence of the incompressibility assumption).

The model domain covers a limited area (5 by 5 km) located in the Kisatchie National Forest on the Fort Polk Military Reservation, about 25 km ESE of

---

*The "buoyancy" referred to in this context [expressed in Eq. (7)] is not a strictly vertical variation because of the terrain-following coordinate system. A horizontal temperature gradient is introduced in this system; thus, a horizontal pressure gradient force appears which is the actual driving mechanism involved in slope flows.

18. Dutton, J.A. (1976) The Ceaseless Wind, McGraw-Hill, New York, pp. 435-439.

Leesville, La. The area consists of rolling hills with tall vegetation.[19] The model makes use of limited meteorological input data (one observation point, using the surface wind, and potential temperatures and geopotential heights at two levels above the surface). The model employs detailed terrain and vegetation data (over a 51-by-51 grid with a grid spacing of 100 m), the latter used to compute surface roughnesses and modify the terrain elevations. The model uses a staggered grid to solve for wind velocity at grid points between the terrain points so that terrain slopes can be computed.

These model characteristics are essentially the same in both ASL and AFGL versions. The modifications made to the ASL model are described in the next section.

2.2 Modifications Made to the Model at AFGL

The ASL windflow model had several computational algorithms that we examined in great detail. The first of these was the determination of surface pressure p_s and "reference" potential temperature θ_o, the latter used as a comparison against a calculated surface potential temperature θ_s for buoyancy determination. In the ASL version of the model, both p_s and θ_o are calculated through a linear extrapolation technique that uses geopotential heights and potential temperatures at two levels above the surface (850 and 700 mb).

We addressed the p_s calculation first. We noted that using a linear extrapolation technique for a nonlinearly varying quantity such as p can lead to errors in the determination of p_s and to subsequent errors in the θ_s calculations. We determined that if a linear extrapolation is used, it should encompass as small a Δp as possible and be done close to the surface. We chose to do the p_s calculations by using geopotential heights at 950 and 900 mb, since these levels are close to the surface over Fort Polk and yield more realistic values of p_s, as illustrated in the example shown in Table 2.

When we addressed the linear extrapolation of θ_o, it became clear that the reference θ_o calculated this way does not represent a true dry adiabatic lapse rate from 850 mb down to the surface. Thus, any buoyancy calculation using this θ_o value is not an accurate estimation of the actual stability conditions. Moreover, similar errors to those in p_s result from extrapolation using θ values at 850 and 700 mb. Since the buoyancy determination in the model determines the stability regime for the surface layer, we felt that the 950-mb potential temperature would be more representative of the average θ in the mixed layer, and that comparing

19. Sadeh, W.Z., Law, F.W., Marlatt, W.E., Fox, D.G., Dietrich, D.L., and Cionco, R.M. (1982) A Survey of Micrometeorological Parameters Within a Forest Canopy at Fort Polk, Louisiana, ASL-CR-0100-1, U.S. Army Atmospheric Sciences Laboratory, White Sands Missile Range, N. Mex.

Table 2. Sample Calculations of p_s Using Linear Extrapolation From 950, 900 mb as Opposed to 850, 700 mb

Standard Formula: $p_s = \frac{p_u - p_L}{h_u - h_L}(h_s - h_L) + p_L$,

where s = surface, u = upper level, and L = lower level.
Let h_s = 75 m (average elevation over Fort Polk), and use climatological $h_{u,L}$ values for January*:

h_{950} = 599 m $\quad$ h_{850} = 1520 m
h_{900} = 1047 m $\quad$ h_{700} = 3115 m

Using 950, 900 mb: p_s = 1008.5 mb

Using 850, 700 mb p_s = 985.9 mb

Using hyposometric eq ($\bar{T}$ = 283.15 K): p_s = 1012.0 mb

*Climatological values for h, T are taken from upper-air data for Lake Charles, La.

this θ_o with θ_s would give a more meaningful estimation of the surface-layer stability than comparison to a linearly extrapolated θ_o using θ from 850 and 700 mb. This point is illustrated in Figure 1. Once this change in the θ_o determination has been made, it is no longer necessary to adjust the buoyancy in the model on the basis of a $\partial\theta/\partial Z$ computation (as is done in the ASL version; see Table 2).

Another change made to the ASL version of the model was the input for determining θ_s and buoyancy. In the ASL version, a surface heating rate ΔQ (based on first law of thermodynamics considerations) is input into the model, and, from it, values of θ_s, T_s (surface air temperature), and buoyancy are determined. We believed that, in an operational scenario, it would be difficult to estimate ΔQ, but T_s is readily available. In the AFGL version, T_s is an input parameter, and it is used to calculate a θ_s field based on the p_s value at each grid point. This θ_s field, when compared with the θ_o field (the latter being a constant field equal to θ_{950}), gives information about the buoyancy as a function of terrain elevation. It should be noted here that the assumption of a constant θ_o field under daytime* conditions is reasonable over a region such as Fort Polk, whose terrain elevations only vary between 60 and 95 m above sea level. However, over a more mountainous region, this assumption should be revised.

*At night, choice of an appropriate θ_o can be difficult because of the formation of the nocturnal inversion. This problem is then complicated by the presence of mountains.

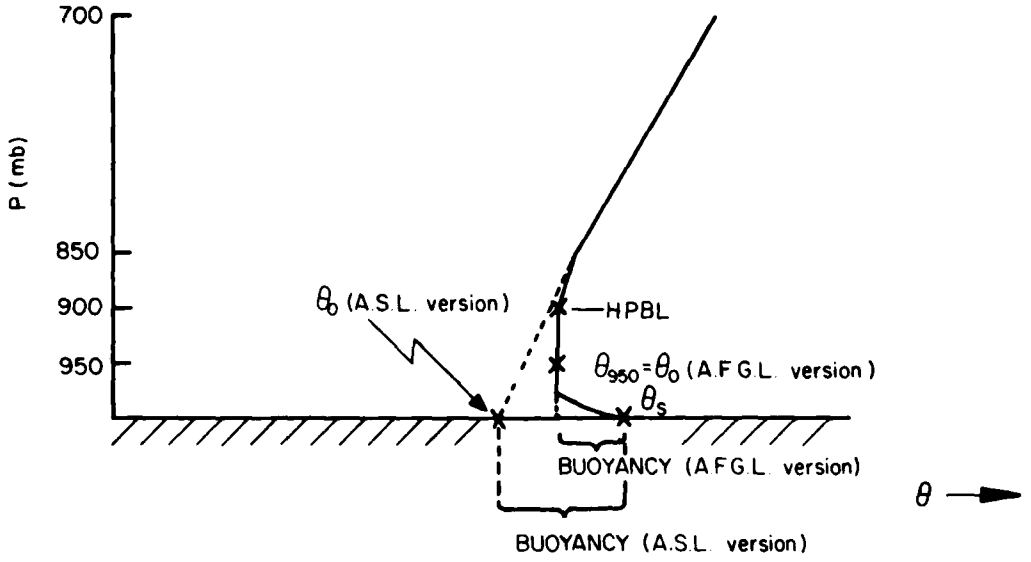

Figure 1. Schematic Diagram Illustrating Differences in Buoyancy Calculation for the ASL and AFGL Versions of the Model. The thick solid line denotes a potential temperature sounding for the unstable case. The dashed line is the calculation of θ_0 by linear extrapolation using θ at 850 and 700 mb. HPBL refers to the planetary boundary layer depth, defined here as the height at which a stable lapse rate is first encountered. In this example, $\theta_0 = \theta_{950}$ (representative of the mean potential temperature in the mixed layer) gives a much more realistic measure of the buoyancy associated with unstable conditions than the linearly extrapolated θ_0 does

Finally, a word should be said about calculation of the bulk Richardson number Ri in the model. The ASL version of the model includes a "curvature" Richardson number based on the effects of flow curvature on stability as documented in a paper by Bradshaw.[20] However, Bradshaw's work was based on physical modeling studies of boundary layers on curved walls, and implies a relationship between temperature fluctuations (producing buoyancy fluctuations) and u-wind component fluctuations (producing Coriolis force fluctuations). A scale analysis of mesoscale atmospheric motions performed by Atkinson[21] shows that, for time and space scales of the order that we are working with for the Fort Polk experiments, the Coriolis force is relatively unimportant. Also, Walmsley[9] says that in the surface layer, the eddy Ekman number is usually much greater than 1, allowing the Coriolis force to be neglected. Thus, we felt that a curvature Ri as included in the ASL model was inappropriate for our work. In several preliminary

20. Bradshaw, P. (1969) The analogy between streamline curvature and buoyancy in turbulent shear flow, J. Fluid Mech. 36, Part 1:177-191.

21. Atkinson, B.W. (1981) Mesoscale Atmospheric Circulations, Academic Press, London, pp. 13-20.

Table 3. Comparison of ASL and AFGL Versions of Model

ASL Version	AFGL Version
Uses 850, 700 mb h, θ for linear extrapolation of p_s, θ_o.	Uses 950, 900 mb h for linear extrapolation of p_s.
Uses linearly extrapolated θ_o as a reference potential temperature against which θ_s is compared to determine value of buoyancy.	Takes θ_{950} and uses it as reference mixed-layer potential temperature θ_o against which θ_s is compared to determine value of buoyancy.
Uses curvature Ri to modify bulk Ri to allow for effects of flow curvature on stability.	Bulk Ri alone is used to determine stability.
Uses surface heating ΔQ as input parameter for calculation of θ_s and T_s.	Uses observed T_s as input and then calculates θ_s from T_s and p_s.
Does an adjustment to θ_s, buoyancy, and Ri to account for lapse rate $\partial\theta/\partial z$ using power law type formulation.	Since buoyancy is calculated based on comparison with potential temperature at 950 mb, no adjustment of θ_s, buoyancy, or Ri is necessary.

experiments with and without this curvature Ri, our hypothesis was confirmed as the flow fields were essentially the same in both experiments (figures not shown).

The major differences between the ASL and AFGL versions of the windflow model are summarized in Table 3.

3. MODEL EXPERIMENTS

This section describes the results of our model evaluation phase. Analysis includes detailed examinations of kinetic energy in the model, and the power law assumption as applied to the wind profiles in the surface layer. We then present the results of our sensitivity experiments.

For the model experiments, we used simulated data based on surface climatology for Fort Polk and upper air climatology for nearby Lake Charles. The simulated data were used to construct soundings representative of the atmosphere for typical January mornings (stable conditions) and July afternoons (unstable conditions). The July afternoon soundings were also used to construct experiments simulating neutral conditions.

3.1 Fort Polk Topography

A detailed description of the Fort Polk topography appears in Sadeh et al.[19] A chart showing the terrain and vegetation over the model domain is shown in Figure 2. Notice from Figure 2 that there are primarily two lowland areas, one running northwest to southeast across the center of the domain (corresponding to Sixmile Creek), and another in the southwest corner of the domain. A ridge runs parallel to the Sixmile Creek lowland area, and high terrain also appears at the northern end. The tallest vegetation over the domain (coniferous trees) averages between 21.3 and 22.5 m high with an average density of 1 tree/4.22 m^2.[19]

Detailed terrain and vegetation data were supplied to us for this area. Although the terrain elevations over this region only varied by 10s of m, the presence of tall vegetation could enhance the complexity of the topography considerably. For instance, a terrain slope from lowland marshes to pine tree-capped hills could be as great as 40 to 50 m over a distance of only several hundred meters. Additionally, the presence of nonhomogeneous vegetation could produce localized "low spots," which could focus the locations of cold pools of air during nocturnal drainage episodes. The model considers the effects of vegetation in two ways: (1) using vegetation heights to modify the terrain elevation, and (2) through the surface roughness. Eq. (5) illustrates the terrain modification by vegetation:

$$h' = h_o + 0.7\, h_{veg}, \tag{5}$$

where h' is the modified terrain height, h_o is the original terrain height, and h_{veg} is the vegetation height. Eq. (5) describes the concept of "displacement length," which is given as being between 70 and 80 percent of h_{veg} and is used to define a height h' to which the logarithmic wind profile can be extrapolated downward from above (see Figure 6.2 in Panofsky and Dutton[22]). The 0.7 h_{veg} term in Eq. (5) agrees well with the 0.68 h_{veg} form proposed by Monteith.[23] Figure 3 illustrates

22. Panofsky, H.A., and Dutton, J.A. (1984) Atmospheric Turbulence: Models and Methods for Engineering Applications, Wiley, New York, pp. 124-125.

23. Monteith, J.L. (1973) Principles of Environmental Physics, Edward Arnold Ltd., London, pp. 88-90.

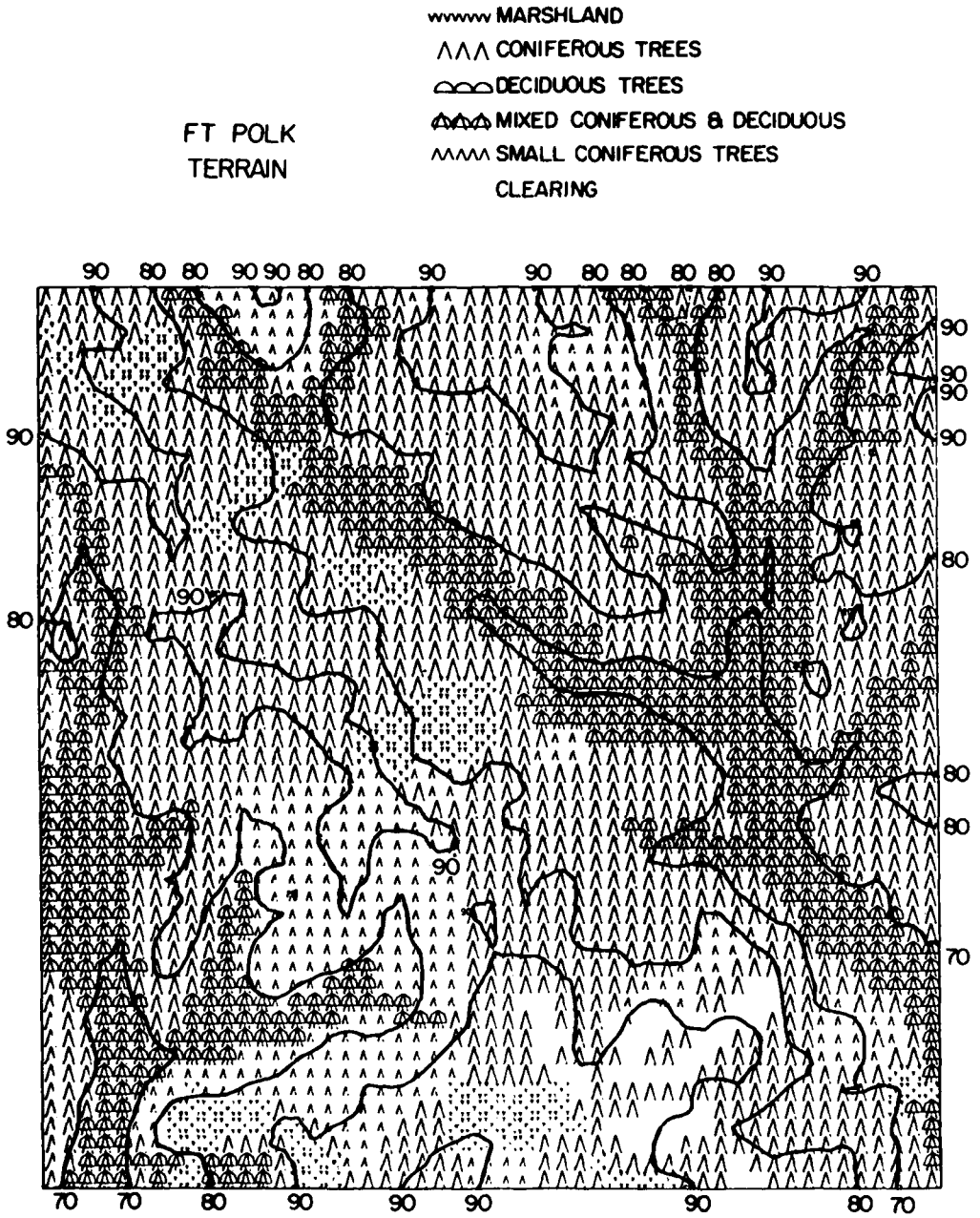

Figure 2. Map of the Model Domain Showing Terrain Elevations (in m) and Vegetation Types. The valley running northwest to southeast across the domain contains Sixmile Creek. Notice that several marshes exist over this valley. These areas will become important when vegetation is added to the terrain heights

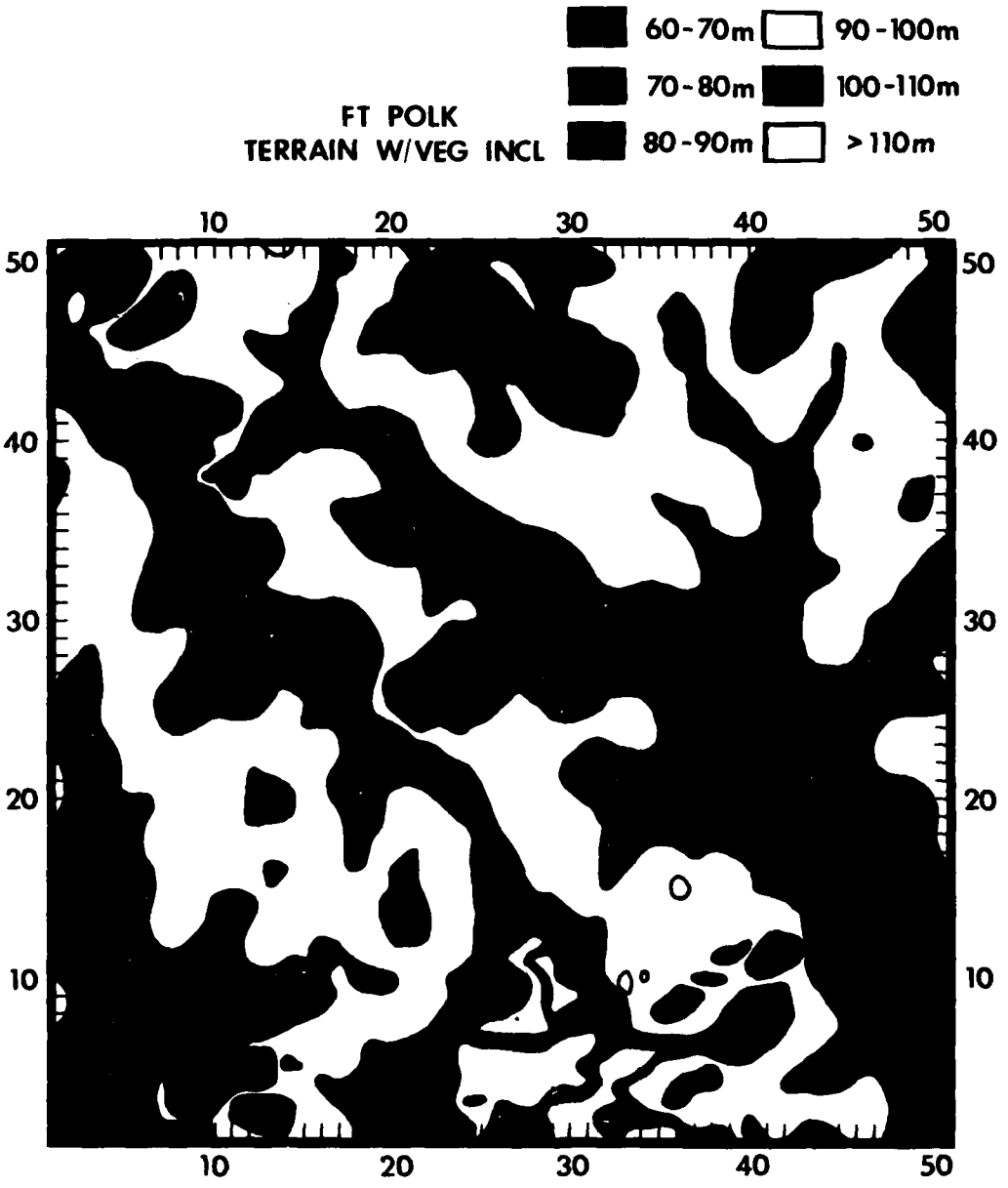

Figure 3. Map of the Model Domain Showing the Terrain Elevations (in m) After Vegetation Heights Are Added

the topography over the domain when Eq. (5) is applied to the terrain elevations. An examination of Figure 3 reveals the appearance of several "low spots" over the domain, with elevations h' less than 80 m. Also, several "peaks" have appeared corresponding to tall pines over high ground, with elevations over 110 m. Additionally, the nonhomogeneity of the terrain has been increased through the addition of vegetation. A comparison of Figures 2 and 3 reveals that the addition of vegetation information to the terrain heights alters the character of the topography over the Fort Polk region.

The second way of considering the effects of vegetation on the topography is through the surface roughness. Many formulations exist for considering roughness as a function of vegetation height (see Monteith,[23] Sellers,[24] and Lettau[25] for discussion of these formulations). In the model, roughness Z_o is computed for each grid point by the following formula:

$$Z_o = 0.14\,(h_{veg} \cdot 0.1). \tag{6}$$

Table 4 shows the Z_o values computed from Eq. (6) for various vegetation types found over the domain. The values of Z_o in Table 4 compare favorably with those

Table 4. Surface Roughness Values Derived From Vegetation Heights

Vegetation Type	h_{veg}(m)	Zo (cm)
Deciduous and Coniferous Trees	21.3	299.7
Coniferous Trees	20.5	288.4
Small Coniferous Trees	14.5	204.4
Marshland	0.9	14.1
Clearing	0.01	1.5

24. Sellers, W.D. (1965) Physical Climatology, U. of Chicago Press, Chicago, pp 150-151.

25. Lettau, H. (1969) Note on aerodynamic roughness-parameter estimation on the bases of roughness-element description, J. Appl. Meteorol. 8:828-832.

obtained using Tanner and Pelton's[26] logarithmic formula, setting a = -0.883 and b = 0.997.

3.2 Analysis of Model Parameterizations

3.2.1 WIND PROFILE SENSITIVITIES TO STABILITY AND ROUGHNESS

The windflow model determines stability through a buoyancy calculation given by the following equation:

$$B = g \frac{\theta_o - \theta_s}{\theta_o}, \tag{7}$$

where g is the gravitational acceleration, $\theta_o = \theta_{950}$ (see Section 2.2), and θ_s is the surface potential temperature. This value of buoyancy is then inserted into the bulk Richardson number calculation, given by Eq. (8) below:

$$Ri = B\, Z/u^2, \tag{8}$$

where $Z = Z_{GRID} + Z_o$ (Z_{GRID} is a reference height = 10 m, in our case), and u is the windspeed at Z. For windspeeds $u \leq 0.1\ ms^{-1}$, the bulk Ri formula is

$$Ri = 100\, BZ. \tag{9}$$

This form of Ri produces large magnitudes of Ri, which explains in part the reason that the model can reproduce topographically driven flows given initially calm wind conditions (see Section 3.3). Determination of Ri defines the stability classification of the surface layer. Seven stability "classes" are used in the model, based on Ri values from -5.0 through 0.25. These stability classes are used to calculate values of the Monin-Obukhov similarity parameters, which help to determine the value of the wind profile exponent n, given by the following relations:

$$n = \begin{cases} [\phi_m / \ln Z/Z_o - \psi'] & , Ri < 0.0 \\ [\phi_m / \ln Z/Z_o + 4.7\,(x - x_o)] & , 0.0 \leq Ri < 0.25 \\ 1 & , Ri \geq 0.25, \end{cases} \tag{10}$$

where ϕ_m is the nondimensional wind shear, ψ' is a Monin-Obukhov function, and

---

26. Tanner, C.B., and Pelton, W.L. (1960) Potential evapotranspiration estimates by the approximate energy balance method of Penman, J. Geophys. Res. 65:3391-3413.

x, x_o are proportional to $(Z/L)^{1/4}$ and $(Z_o/L)^{1/4}$, respectively [see Eqs. (2.30 a-d)] in Amlicke and Coleman.[16]

The model makes use of the Businger et al[27] wind profiles by assuming that they can be applied locally at each grid point.[4] The wind profile exponent is used in a power law formation to evaluate the wind at the computation height Z_c (top of the flux box). The values of ϕ_m used in the model are the same as those of Businger et al and are not directly influenced by different Z_o values (see Figure 4).

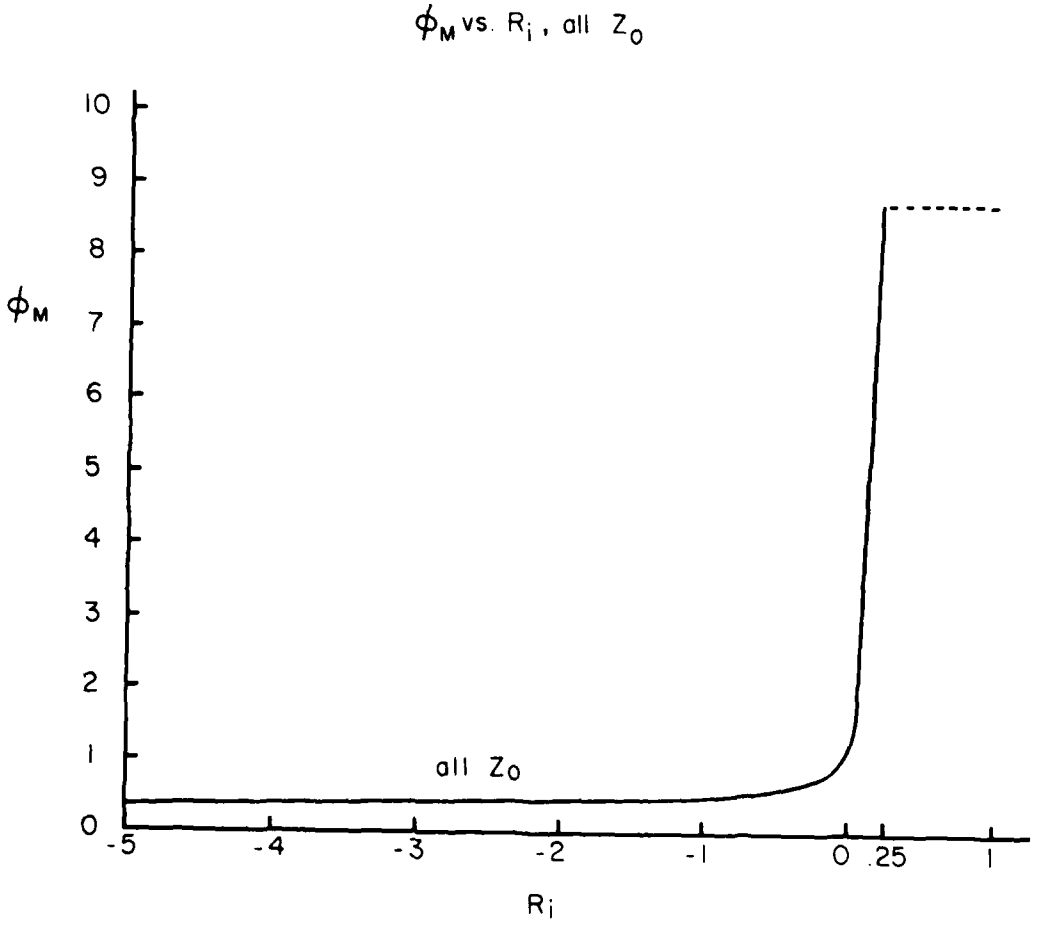

Figure 4. Graph of ϕ_m (Non-Dimensional Wind Shear) as a Function of the Bulk Richardson Number Ri, for All Values of Surface Roughness Z_o

---

27. Businger, J.A., Wyngaard, J.C., Izumi, Y., and Bradley, E.F. (1971) Flux-profile relationships in the atmospheric boundary layer, J. Atmos. Sci, 28:181-189.

However, the value of n is sensitive to the roughness, as illustrated by the graph of Figure 5. Figure 5 shows the value of n increases with increasing Z_o. Thus, it is possible for roughness effects to feed back to the windfield during the model integration and alter the stability of the surface layer.

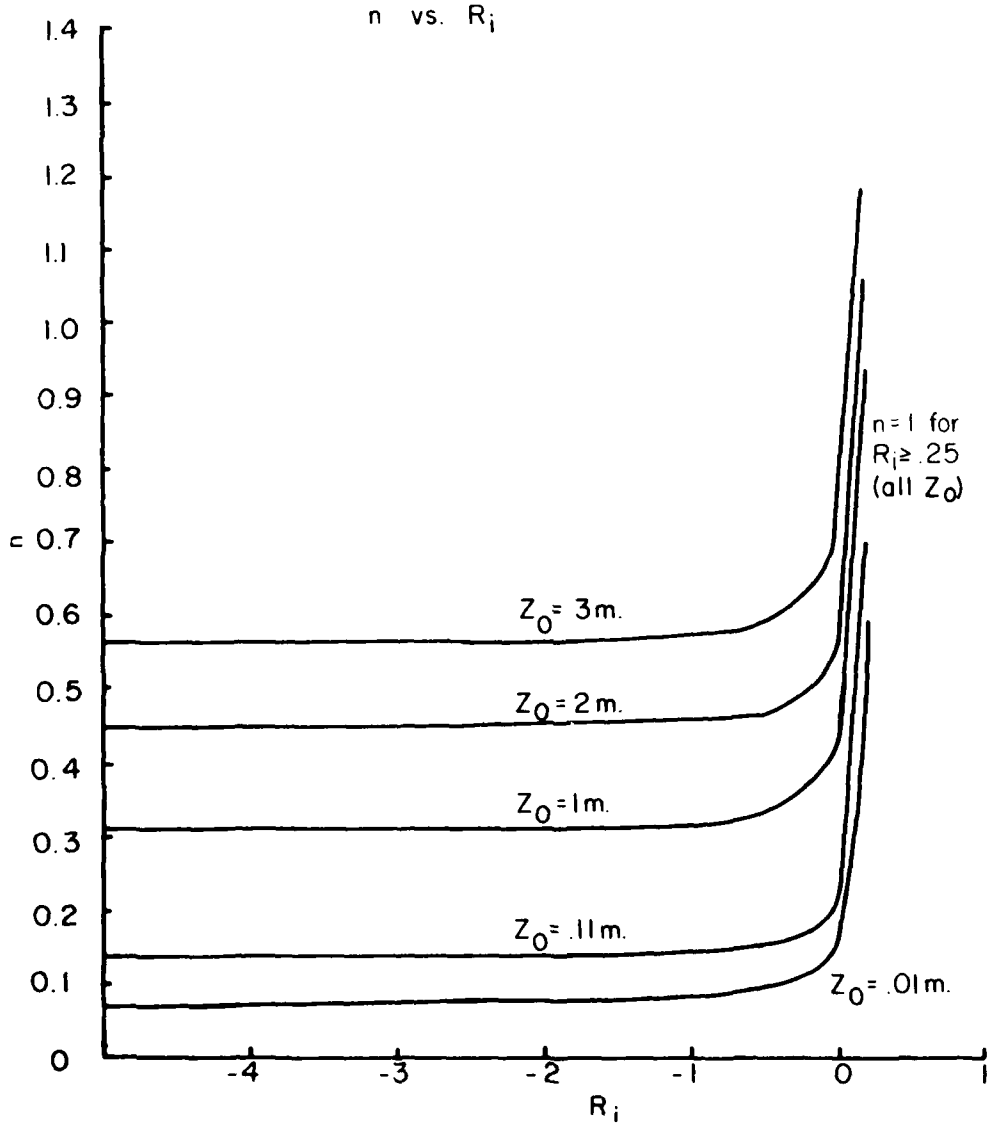

Figure 5. Graph of Wind Profile Exponent n as a Function of Bulk Richardson Number Ri, for Different Values of Surface Roughness Z_o

3.2.2 ANALYSIS OF MODEL KINETIC ENERGY

The basic model Eq. (1) describes the adjustment of an initially uniform windfield (based on a single input observation) to conform with buoyancy and topography. During this adjustment, the integral residual R must be continually decreasing until a quasi-steady state balance is achieved and the value of R reaches a minimum. Since the buoyancy essentially remains the same throughout the model relaxation, it follows that a considerable adjustment in the total domain kinetic energy KE takes place during this time.

We studied the changes in total KE during the model integrations in detail, examining sensitivity to stability (that is, buoyancy), initial wind speed, and number of model iterations. Our results can be summarized by the following statements:

(1) KE is sensitive to the magnitude of the buoyancy in the model. Final KE is higher for larger magnitudes of buoyancy. KE decreases through the integration for the neutral case.

(2) KE is sensitive to the initial wind speed. When initially low ($2\,ms^{-1}$) wind speeds are used, the KE tends to increase through the integration. When the initial wind speeds are high ($10\,ms^{-1}$), KE decreases through the integration.

(3) The model wind field essentially reaches quasi-steady state after 60 iterations.

We will now address each of these results individually.

The first result makes sense when one examines Eq. (1), since the winds in the acceleration term would have to be stronger to adjust to a stronger value of B in the integral. This point is further addressed in Section 3.3. The sensitivity of the model KE to buoyancy is illustrated by the graphs in Figure 6, which show the change in KE as a function of the number of iterations NR. Note that in the experiment with B = -0.06 (slightly unstable), the KE actually decreases slightly during the model integration. This occurs because of the small magnitude of buoyancy used in that experiment. The experiment with B = -0.18 (moderately unstable), which also shows a decrease in KE, is one in which an initial wind speed of $10\,ms^{-1}$ was used. An initial windspeed of $10\,ms^{-1}$ was also used for the neutral case (B 0 curve in Figure 6). The results from Figure 6 suggest that there exists some intermediate wind speed between 2 and $10\,ms^{-1}$ for which KE would remain fairly constant through the model integration. As far as the third result is concerned, notice that Figure 6 shows the KE changes for four experiments which were integrated to NR 200. A total of eight experiments were actually run with NR = 200, and the results of these experiments indicated that, at NR = 60, KE reached roughly 65 percent of its value at NR = 200. This percentage also appears to be sensitive to the magnitude of the buoyancy, as shown in Figure 6.

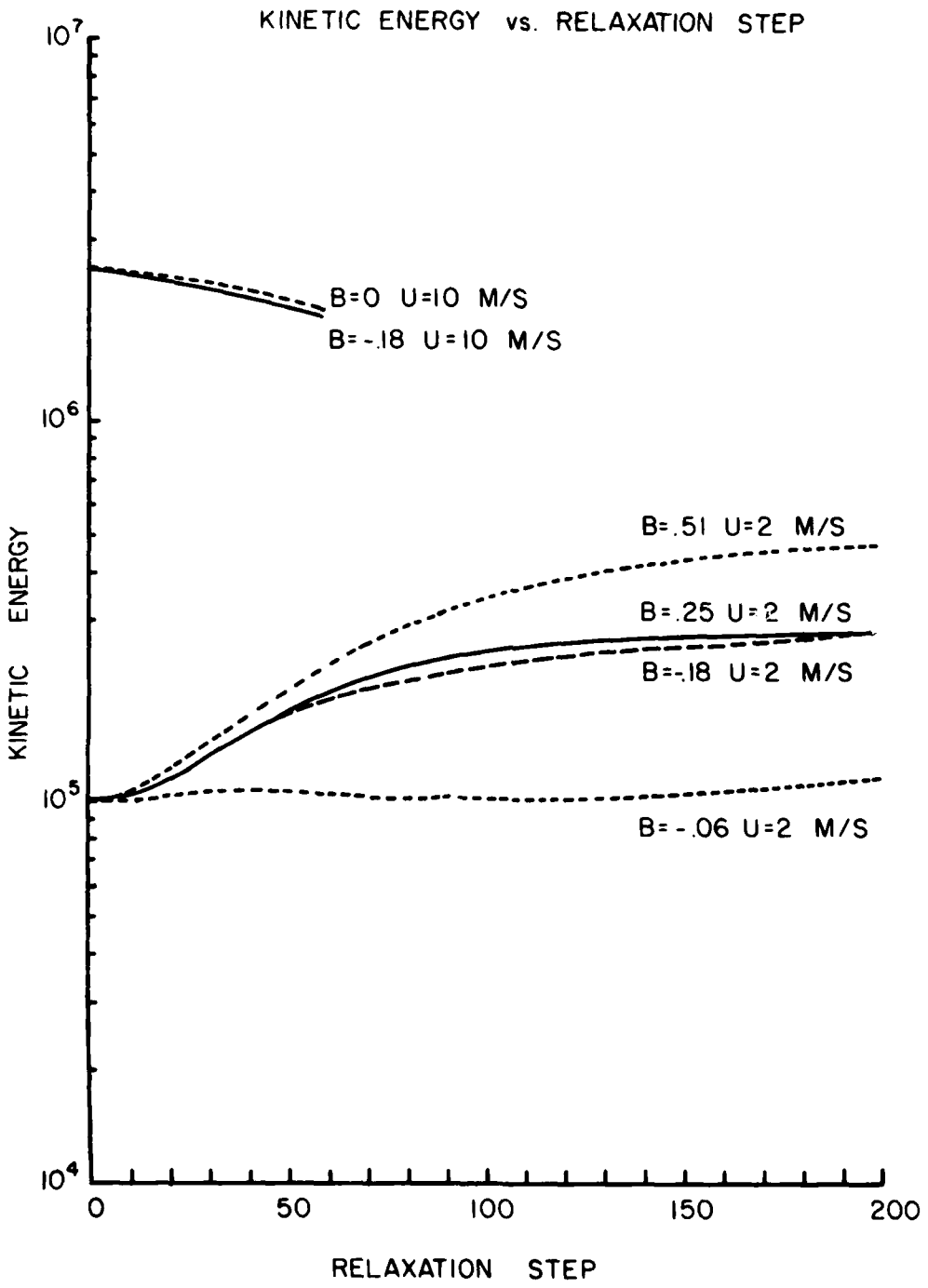

Figure 6. Change in Total Model Kinetic Energy KE as a Function of the Number of Model Iterations, NR, for Different Values of the Surface-Layer Buoyancy B and Initial Wind Speed u

However, a comparison of the wind fields produced at NR = 60 with those at NR = 200 (figures not shown) reveals that the flow patterns fully develop in the model by NR = 60.

3.3 Windflow Characteristics Under Various Stability Conditions

This section documents our results from the model sensitivity experiments with and without vegetation. The formulation of soundings simulating stable, unstable, and neutral conditions was described at the beginning of Section 3. The climatological soundings for the two stable cases are shown in Figure 7a. Two soundings each were formulated for this and the unstable case to test the model sensitivity to the magnitude of the buoyancy. Similar soundings for the unstable cases are shown in Figure 7b. The neutral case sounding is shown in Figure 7c.

Climatology for Fort Polk indicated that the preferred wind direction and speed during January mornings (0600-0800 LST) was from the north at 2.3 ms^{-1} (although calm actually has the highest frequency for this time). The southerly direction was the second most frequent direction, and this direction was chosen for the sensitivity tests to allow direct comparisons with the unstable cases. For July afternoons (1500-1700 LST), south was the preferred direction with a mean speed of 3.0 ms^{-1}. Calm had the second highest frequency at this time.

Table 5 gives the input information used to initialize the model for the eight experiments that tested model sensitivity to stability and wind conditions. It should be noted here that experiments were run for the model using other wind directions, and the results were consistent with the model physics and results using a southerly wind.

The model domain for the experiments with vegetation appeared in Figure 3, and the domain for the experiments without vegetation appeared in Figure 2. The model runs made using the vegetation information employed horizontally varying roughness. The experiments with no vegetation used a horizontally uniform roughness of 14 cm, corresponding to h_{veg} = 0.9 m (rolling hills with tall grasses). This value of Z_o was chosen in order not to be on the lowest wind exponent curve (see Figure 5), yet realistically simulate a lack of tall vegetation in the area.

A problem exists when trying to interpret results from experiments using no vegetation and uniform Z_o. The problem is how to isolate the effects on the flow field of vegetation alone from those caused by variable roughness alone. To solve this problem, model runs were made where the effects of vegetation on the terrain heights were maintained, but a uniform Z_o of 14 cm was used. These results could be compared with results from model runs using vegetation and variable Z_o to isolate the effects on the windfield of variable roughness alone. These comparisons revealed that the effects of horizontally varying roughness are minimal.

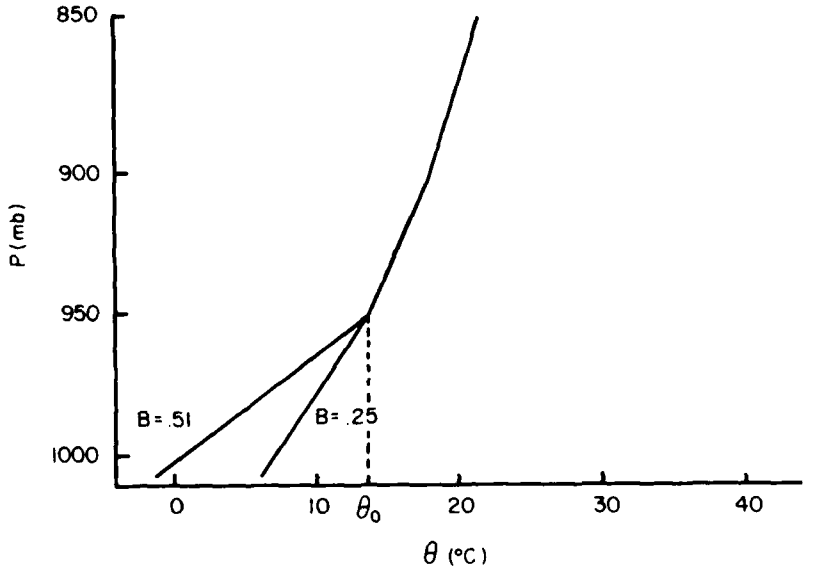

Figure 7a. Climatological Soundings of Potential Temperature for Stable Conditions for Fort Polk Model Runs. Dashed line denotes value of $\theta_0 = \theta_{950}$. Buoyancy values are displayed next to each sounding

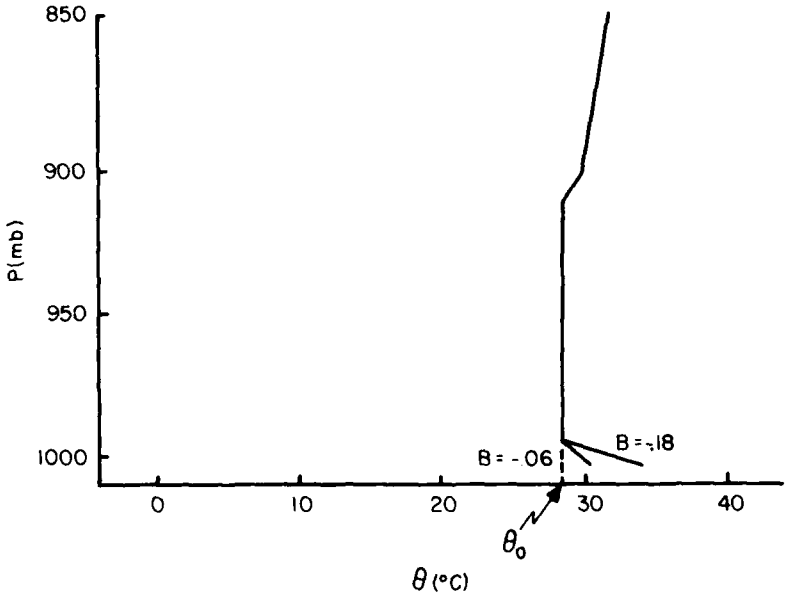

Figure 7b. Climatological Soundings of Potential Temperature for Unstable Conditions for Fort Polk Model Runs. Dashed line denotes value of $\theta_0 = \theta_{950}$. Buoyancy values are displayed next to each sounding

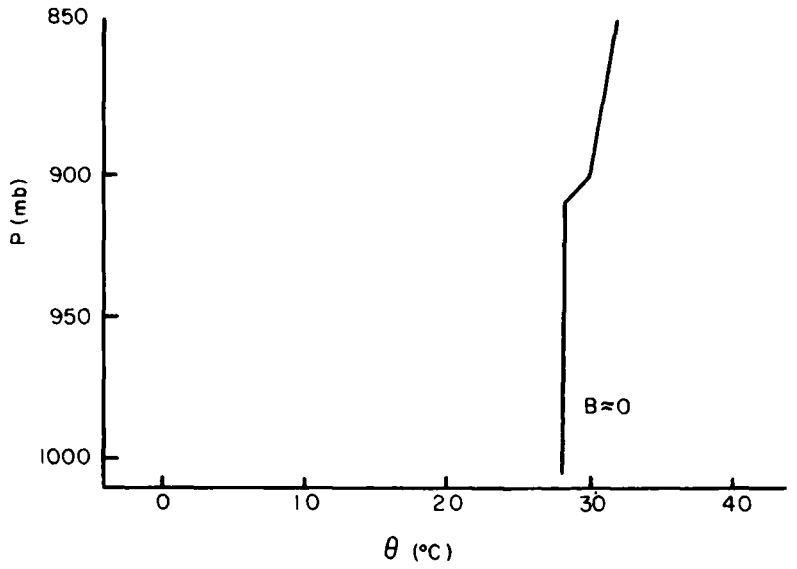

Figure 7c. Climatological Sounding of Potential Temperature for the Neutral Condition for Fort Polk Model Runs. Buoyancy value is displayed next to the sounding

Table 5. Input Data for Model Experiments

Experiment No. **	Wind Dir	Speed (ms^{-1})	T_s (°C)	θ_o (°C)	B*(ms^{-2})
1 (stable)	S	2	7.2	13.9	0.25
2 (very stable)	S	2	-0.4	13.9	0.51
3 (slightly unstable)	S	2	30.6	28.3	-0.06
4 (very unstable)	S	2	34.4	28.3	-0.18
5 (very unstable)	S	10	34.4	28.3	-0.18
6 (neutral)	S	10	28.7	28.3	0.00
7 (very stable)	Calm		-0.4	13.9	0.51
8 (very unstable)	Calm		34.4	28.3	-0.18

*Values of B based on θ_s values calculated using p_s (Jan) = 1007.4 mb and p_s (July) = 1004.0 mb.

**Experiments using no vegetation, with uniform roughness of 14 cm are numbered the same as below with a suffix "a."

The flow patterns remained essentially the same, with the upslope and drainage flows nearly identical in experiments with and without nonuniform roughness (figures not shown). One curious result of the comparison was that the total KE over the domain averaged about 13 percent less for the uniform Z_o cases than for the varying Z_o cases. We believe these differences to be rather small, considering the total grid size involved (50 by 50 grid; 2500 grid points). These results suggest that the model runs using vegetation and nonuniform roughness can be directly compared with experiments using no vegetation and uniform roughness, because the effects of variable roughness are second-order.

3.3.1 STABLE CONDITIONS WITH VEGETATION

The stable surface layer was simulated in experiments 1, 2, and 7. The input data for these experiments are shown in Table 5. In experiments 1 and 2, the input wind speed of 2 ms^{-1} is close to the climatological value of 3.5 ms^{-1} for this direction in January.

Figure 8a shows the windfield for experiment 1. Notice that there are several convergence zones corresponding to cold air drainage into low spots on the domain. The model is capable of simulating cold air drainage off the higher terrain and flow diversion around terrain obstacles such as hills and ridges. When the buoyancy is increased (experiment 2; Figure 8b), the windfield is essentially the same except for some weakening of the flow over the level terrain areas and some enhancement of the slope winds in the drainage areas. The enhancement of the slope flow occurs because of the model response to buoyancy and topography. Recall from Section 2 that the surface layer is divided into flux boxes of thickness Z_c and that these boxes are distorted to conform with the terrain slopes. Also recall from Section 3.2.2 that model KE was larger for experiments with larger magnitudes of buoyancy. At this point in our evaluation, it is too early to verify this slope-flow enhancement against observations, although these results are inconsistent with the numerical results of McNider and Pielke[28] and analytical results of McNider.[29]

The model is also capable of generating cold air drainage flows given initially calm wind conditions. This result is illustrated in Figure 8c, which shows the model windfield for experiment 7. Notice that the drainage is focused into low-lying areas (lowland marshes along Sixmile Creek), and that the strongest drainage occurs over the steepest terrain slopes. Again, these results are consistent with the constraint Eq. (1).

---

28. McNider, R.T., and Pielke, R.A. (1984) Numerical simulation of slope and mountain flows, J. Climate and Appl. Meteorol. 23:1441-1453.

29. McNider, R.T. (1982) A note on velocity fluctuations in drainage flows, J. Atmos. Sci. 39:1658-1660.

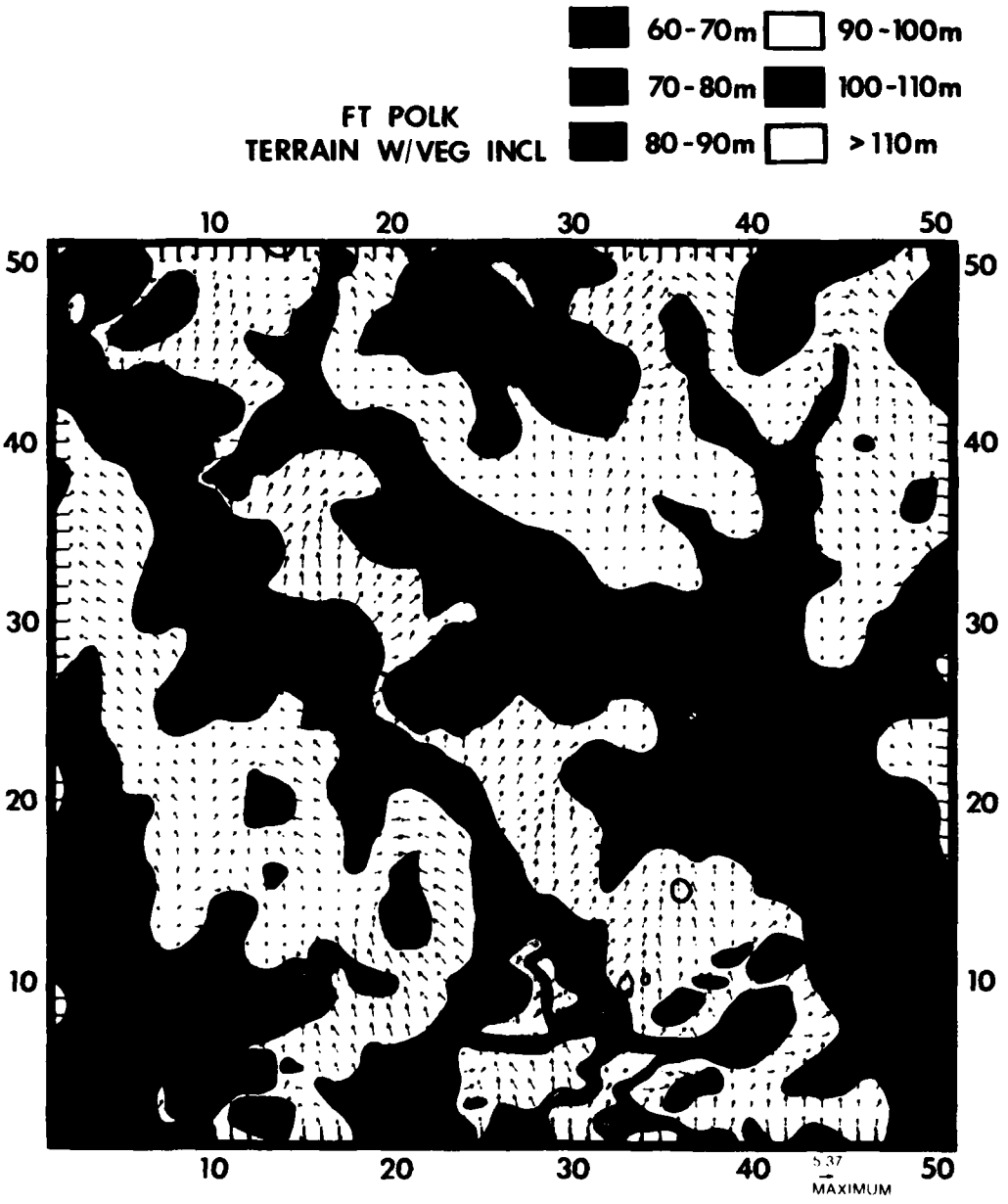

Figure 8a. Model Windfield for Experiment 1 Showing Wind Velocity Vectors for Stable Case With Vegetation (Length Proportional to Speed; See Maximum Vector Displayed in Lower Right). Terrain elevations are highlighted as in Figure 3

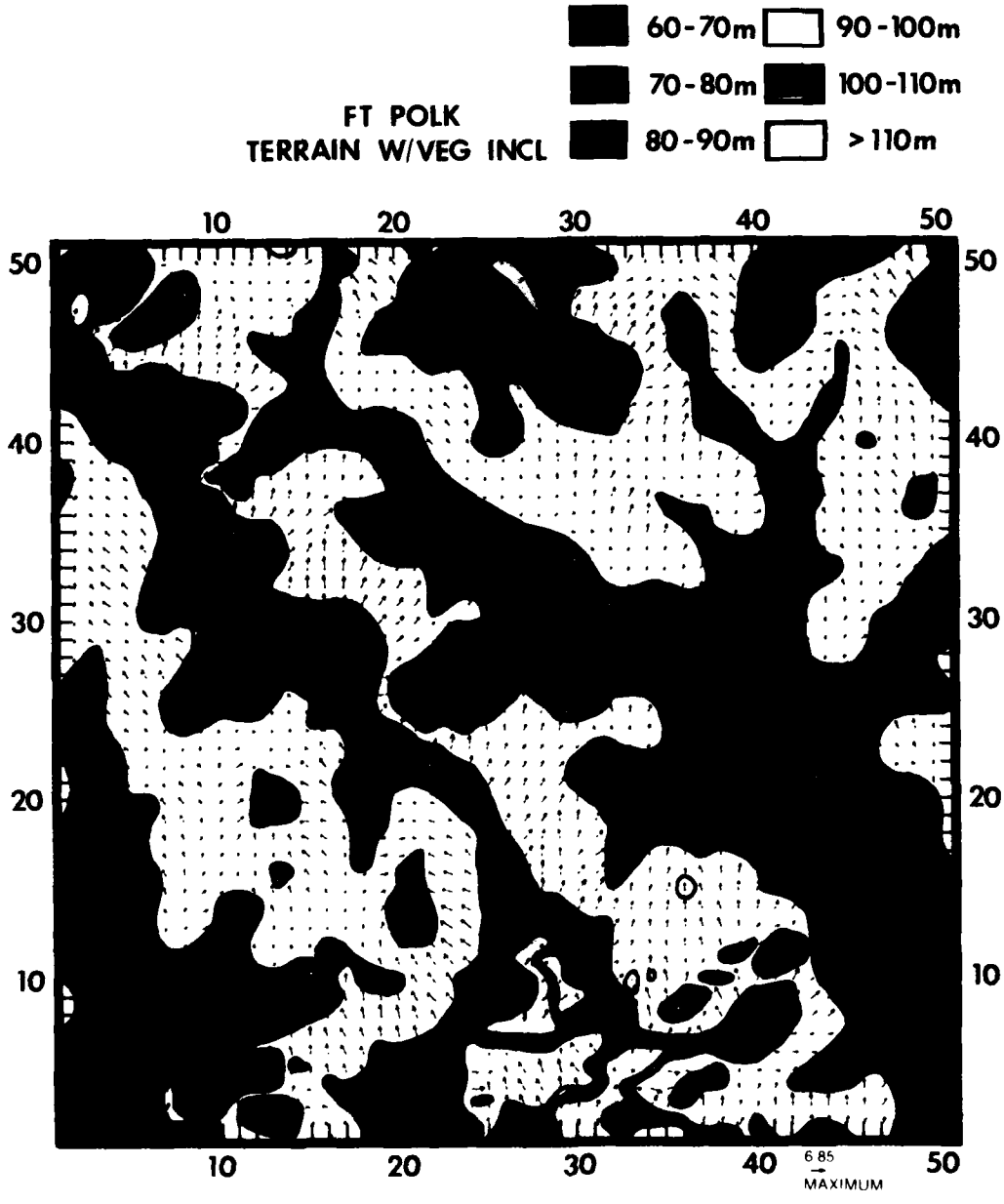

Figure 8b. Model Windfield for Experiment 2 Showing Wind Velocity Vectors for Stable Case With Vegetation (Length Proportional to Speed; See Maximum Vector Displayed in Lower Right). Terrain elevations are highlighted as in Figure 3

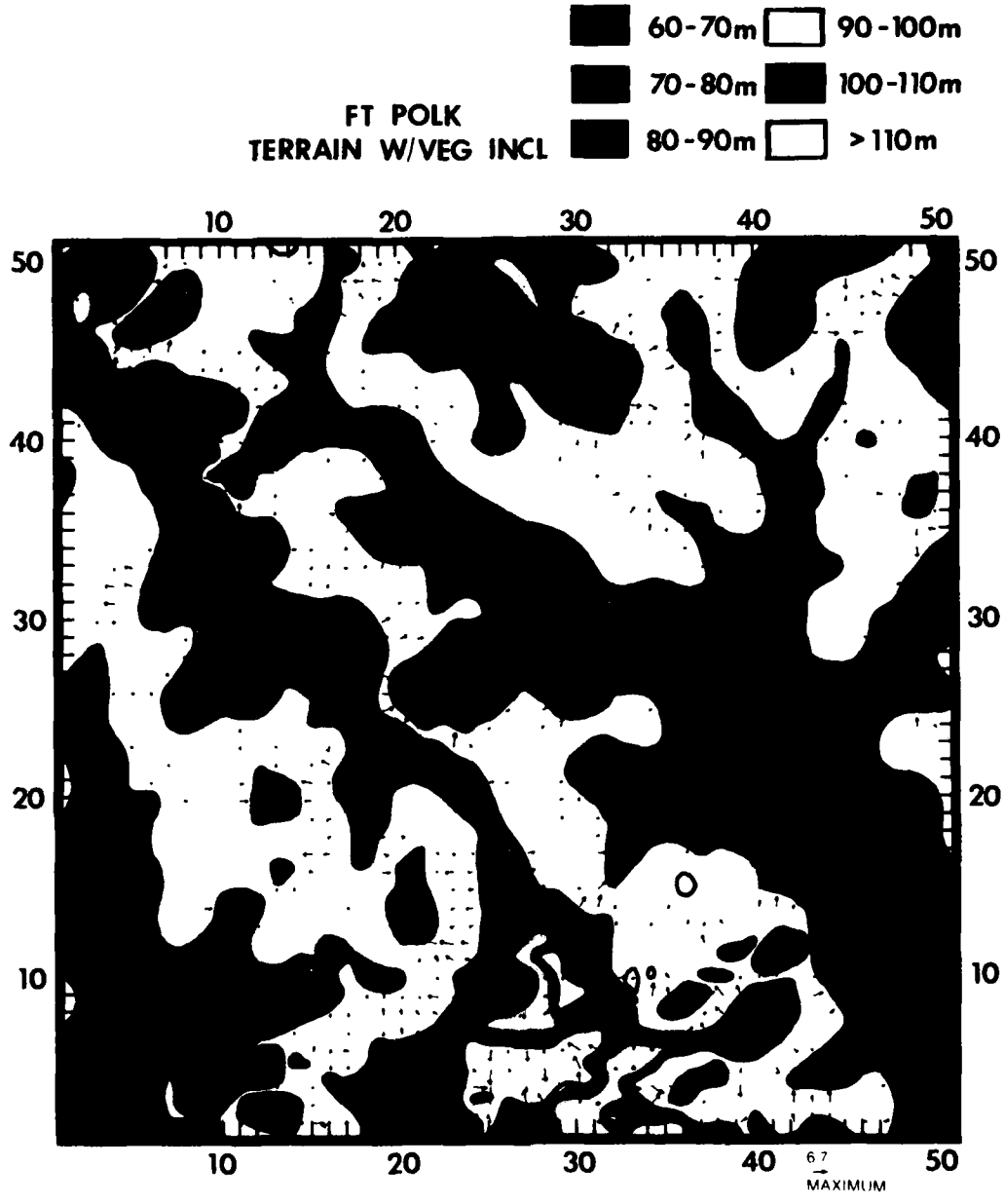

Figure 8c. Model Windfield for Experiment 7 Showing Wind Velocity Vectors for Stable Case With Vegetation (Length Proportional to Speed; See Maximum Vector Displayed in Lower Right). Terrain elevations are highlighted as in Figure 3

3.3.2 UNSTABLE CONDITIONS WITH VEGETATION

The experiments simulating unstable conditions were experiments 3, 4, 5, and 8. In experiments 3 and 4, the input wind speed of 2 ms^{-1} corresponds closely to the climatological value (3 ms^{-1}). Use of the same wind speeds (2 ms^{-1} in experiments 3 and 4) enables us to make comparisons of these experiments with those for the stable cases.

The windfield for the slightly unstable case (experiment 3) is shown in Figure 9a. Notice that, for this case, the model produces upslope flows and ridgetop convergence over areas of high terrain. When the magnitude of the buoyancy is increased (experiment 4; Figure 9b), the upslope flows are enhanced, and some of the convergence patterns along the higher terrain are sharper. As with the stable case, the model is capable of simulating topographically induced flows given initially calm winds. This is illustrated by the windfield of experiment 8 (Figure 9c). As in experiment 7, the strongest slope flows nearly coincide with the steepest terrain slopes.

All of the experiments discussed so far have been run using small initial windspeeds. With such light winds, it would be expected that topographically induced flows would be the dominant features. The question then arises, What if higher winds prevailed over the area? One would expect the stronger winds to dominate the topographic flows. This is demonstrated in experiment 5 (Figure 9d), which shows a fairly uniform windfield only slightly influenced by topography. An unstable, high wind speed case can exist for situations where vertical mixing of strong momentum from aloft begins to occur after breakdown of the nocturnal inversion. It has been shown over mountainous regions that, once this strong mixing has begun, topographically induced flows begin to disappear and are replaced by strong uniform wind conditions at the surface.[30,31]

3.3.3 NEUTRAL CONDITIONS WITH VEGETATION

Neutral conditions were simulated using the July climatological sounding (Figure 7c; Table 5). The windfield for this case is shown in Figure 10. The results are as expected: fairly uniform winds with only slight influence from the topography. To verify that the uniform windfield was caused only by the neutral surface layer and not by the initial wind speed of 10 ms^{-1}, an additional experiment was run with neutral conditions and an initial wind speed of 2 ms^{-1}. Results of this experiment (not shown) revealed that the uniform windfield was indeed caused

---

30. Banta, R.M. (1982) An Observational and Numerical Study of Mountain Boundary-Layer Flow, Ph.D. thesis, Colorado State U., Ft. Collins, Colo.

31. Banta, R.M. (1984) Daytime boundary-layer evolution over mountainous terrain. Part I: Observations of the dry circulations, Mon. Wea. Rev. 112:340-356.

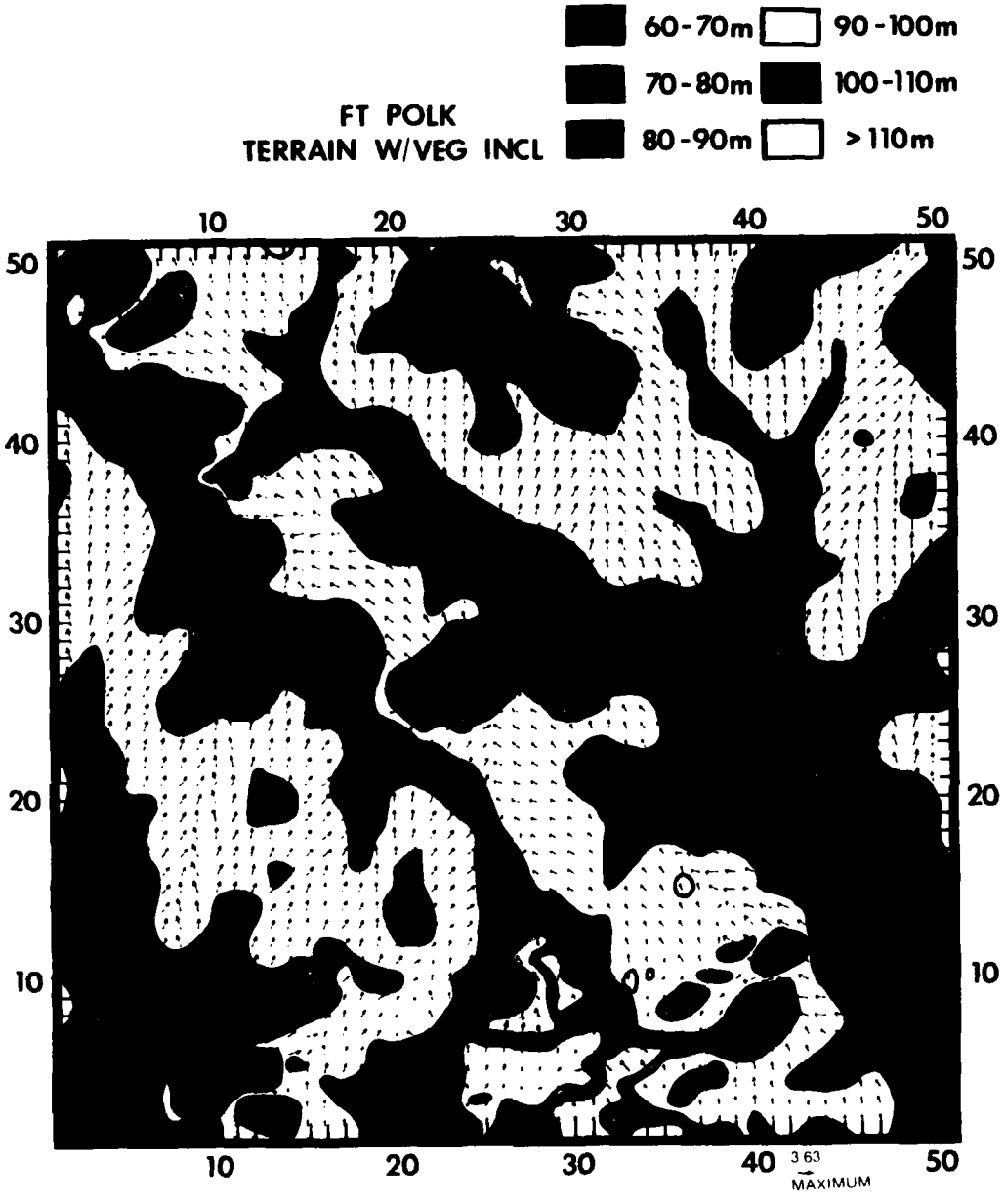

Figure 9a. Model Windfield for Experiment 3 Showing Wind Velocity Vectors for Unstable Case With Vegetation (Length Proportional to Speed; See Maximum Vector Displayed in Lower Right). Terrain elevations are highlighted as in Figure 3

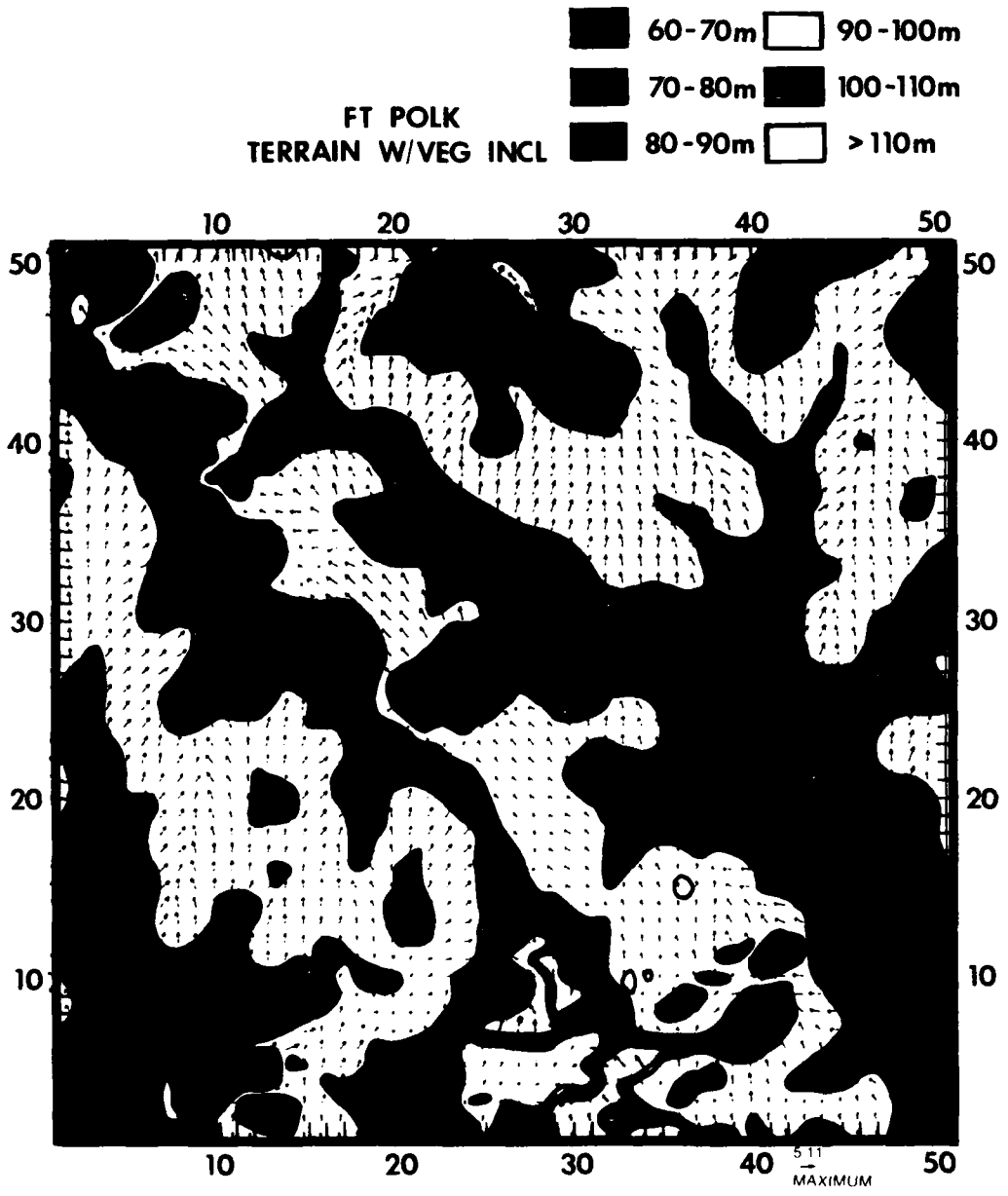

Figure 9b. Model Windfield for Experiment 4 Showing Wind Velocity Vectors for Unstable Case With Vegetation (Length Proportional to Speed; See Maximum Vector Displayed in Lower Right). Terrain elevations are highlighted as in Figure 3

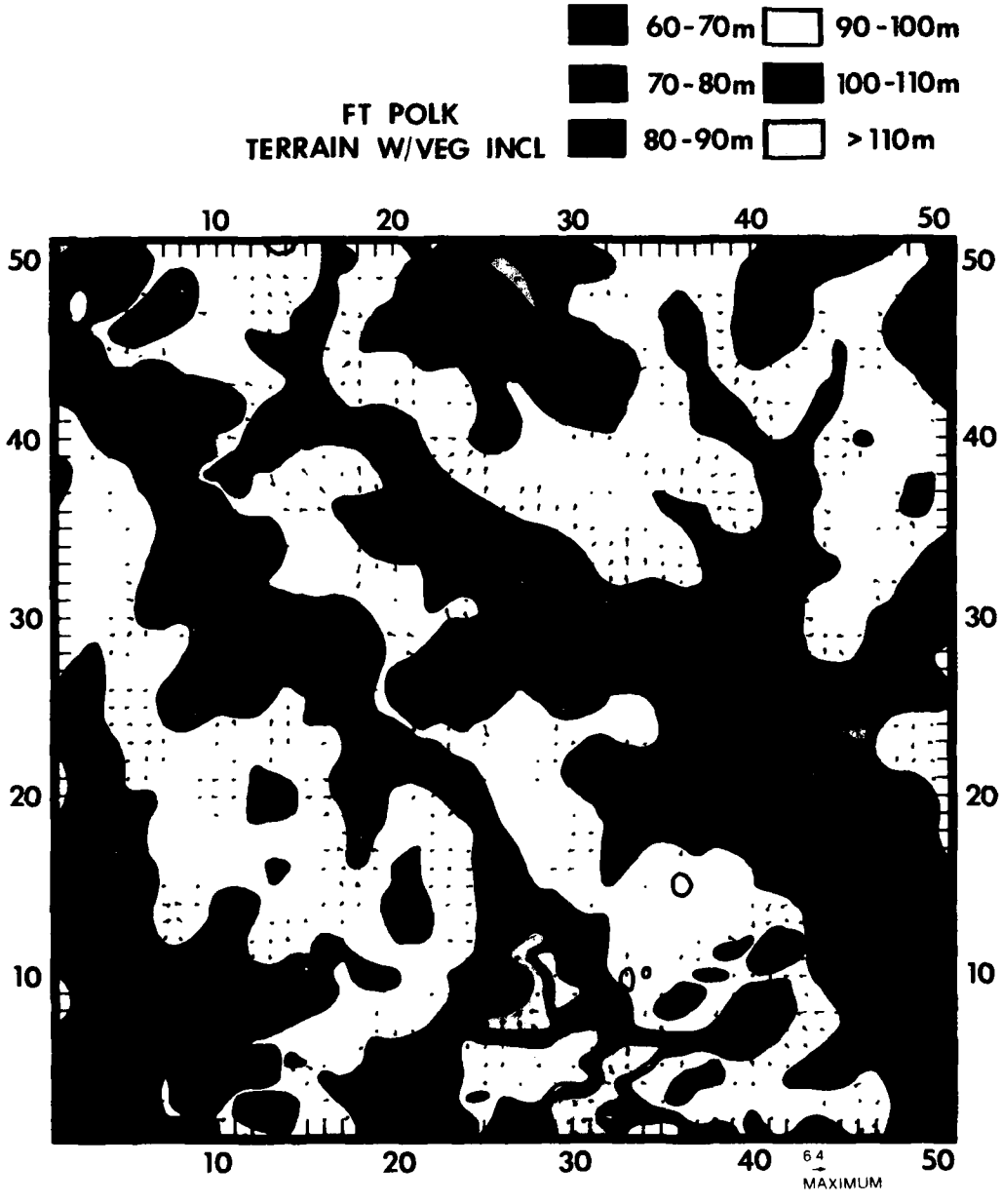

Figure 9c. Model Windfield for Experiment 8 Showing Wind Velocity Vectors for Unstable Case With Vegetation (Length Proportional to Speed; See Maximum Vector Displayed in Lower Right). Terrain elevations are highlighted as in Figure 3

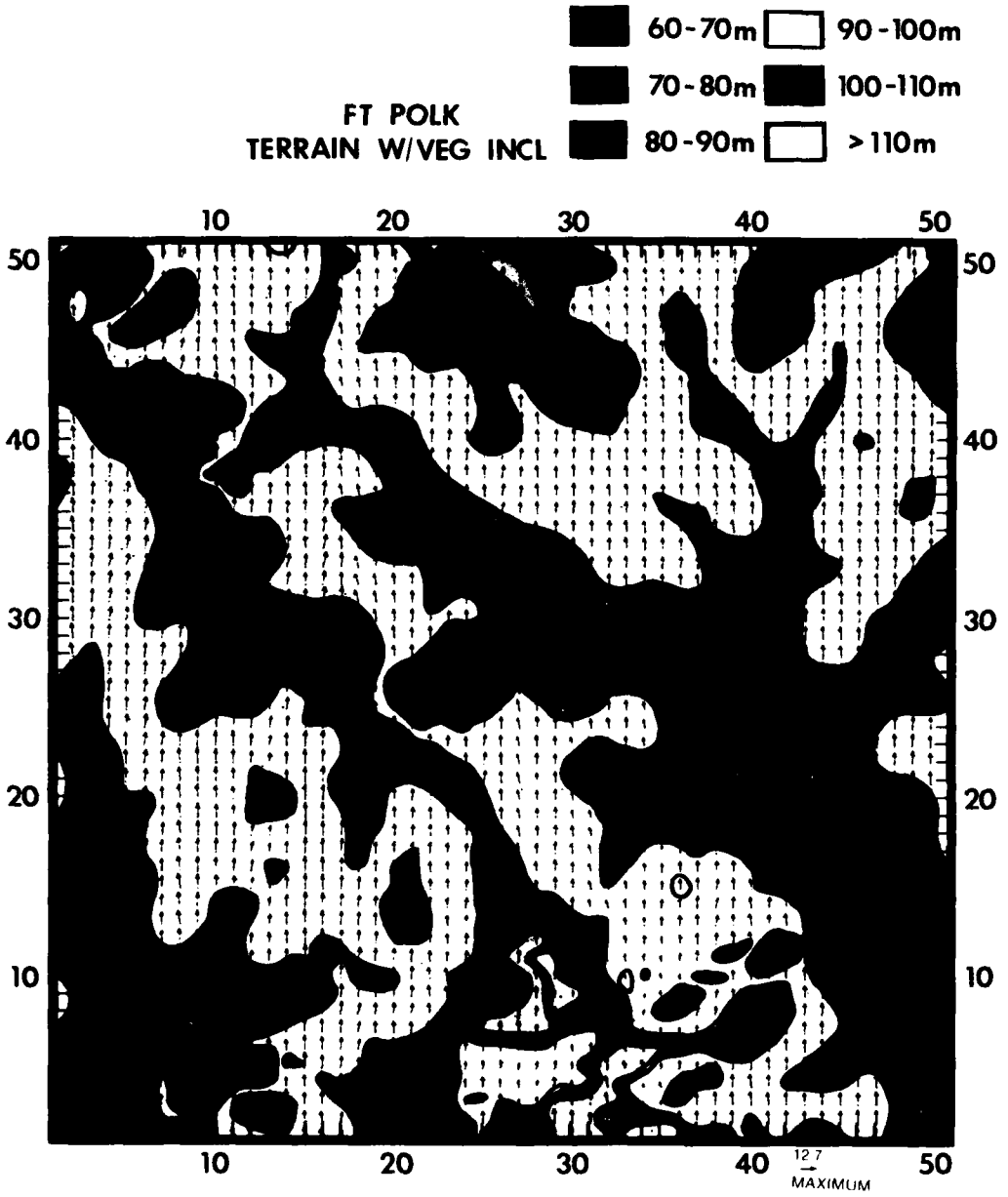

Figure 9d. Model Windfield for Experiment 5 Showing Wind Velocity Vectors for Unstable Case With Vegetation (Length Proportional to Speed; See Maximum Vector Displayed in Lower Right). Terrain elevations are highlighted as in Figure 3

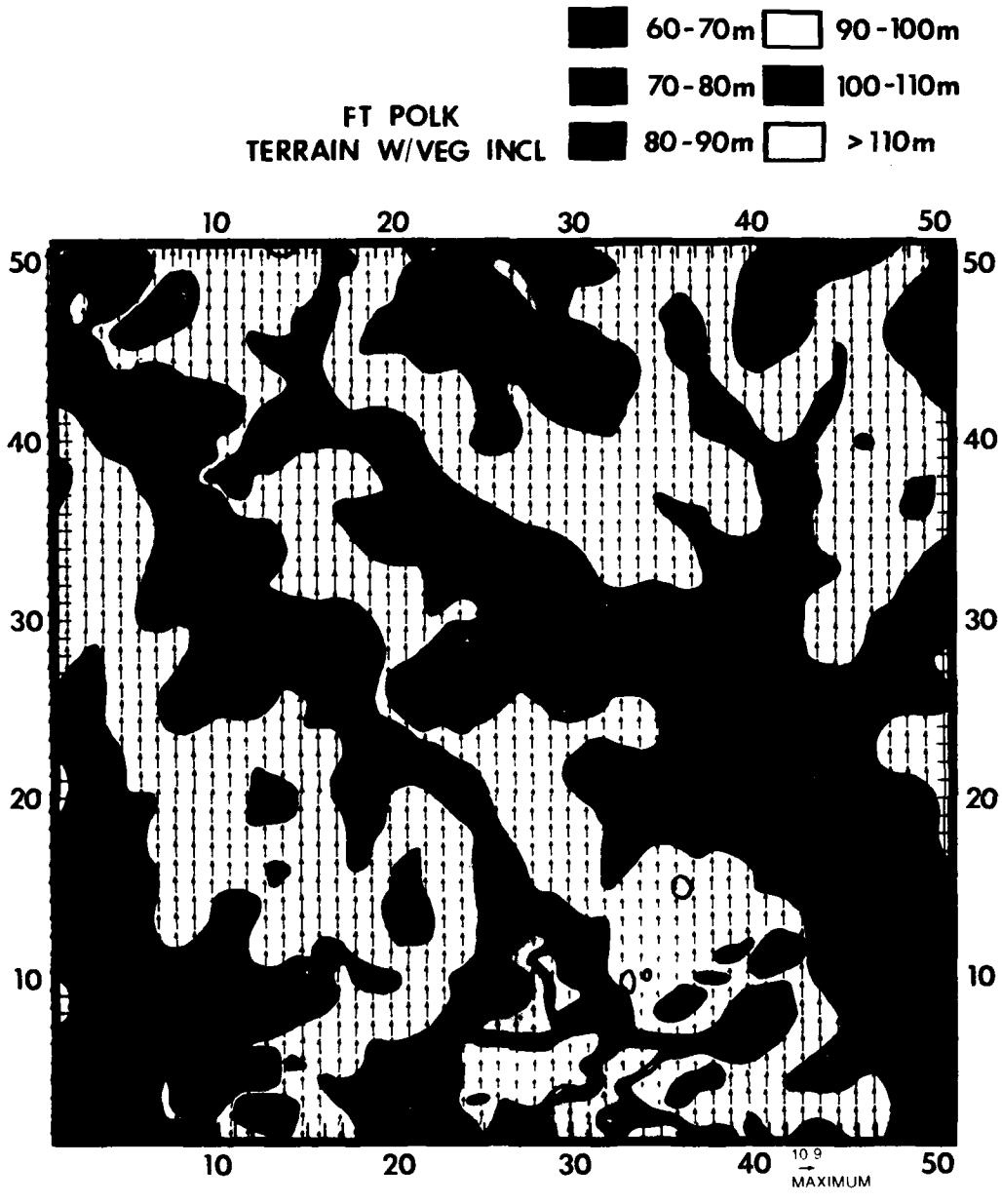

Figure 10. Model Windfield for Experiment 6 Showing Wind Velocity Vector for Neutral Case (Length Proportional to Speed; See Maximum Vector Displayed in Lower Right). Terrain elevations are highlighted as in Figure 3

by the neutral conditions. Notice from Figure 10 that speed-up of the wind occurs downwind of some of the low spots in the terrain. Speed-up has been theoretically related to terrain geometry (see Orgill[32] for a short review of the work done on the speed-up factor), so it is not surprising that the model is capable of reproducing this phenomenon, if somewhat crudely.

3.3.4 STABLE CONDITIONS WITHOUT VEGETATION

Experiments simulating the stable surface layer without vegetation and with uniform surface roughness of 14 cm are experiments 1a, 2a, and 7a. Results from experiment 1a are shown in Figure 11a. Downslope flow corresponding to cold air drainage appears in this experiment. Notice the uniformity in the drainage flow along the NW-SE axis of the Sixmile Creek valley; the drainage flow appears to describe a "downslope front" coming off the ridge. Contrasting this flow field with the one in experiment 1 (same conditions, except with vegetation and variable surface roughness; see Figure 8a) reveals that the addition of vegetation disrupts the uniformity of the downslope front, concentrating the drainage instead into localized low spots corresponding to the lowland marshes. These results have significant implications in the area of toxic chemical diffusion. The presence of nonhomogeneous vegetation can alter the flow field and subsequently alter the chemical transport and diffusion, perhaps focusing high concentration levels into these localized lowland areas under stable conditions.

When the buoyancy is increased (experiment 2a), similar effects take place as occurred in the stable cases with vegetation (experiment 2). The windfield for experiment 2a is omitted here for that reason. An experiment simulating stable conditions with initially calm winds (experiment 7a) was conducted, and the windfield is shown in Figure 11b. Notice that the downslope flow appears over different parts of the domain than it does in the same case with vegetation (experiment 7; Figure 8c). This is a further illustration of the effects of nonhomogeneous vegetation on drainage flows, again with important implications on the transport and diffusion problem.

3.3.5 UNSTABLE CONDITIONS WITHOUT VEGETATION

Experiments 3a, 4a, 5a, and 8a were simulations using unstable conditions with no vegetation, and with uniform roughness of 14 cm. The windfield for experiment 3a appears in Figure 12a. Notice the upslope flows and ridgetop convergence simulated by the model in this experiment, consistent with the results of the same case with vegetation (experiment 3; Figure 9a). However, the windfield

---

32. Orgill, M. M. (1981) Atmospheric Studies in Complex Terrain: A Planning Guide for Future Studies, PNL-3656, ASCOT/80/4, Pacific Northwest Laboratory, Richland, Wash.

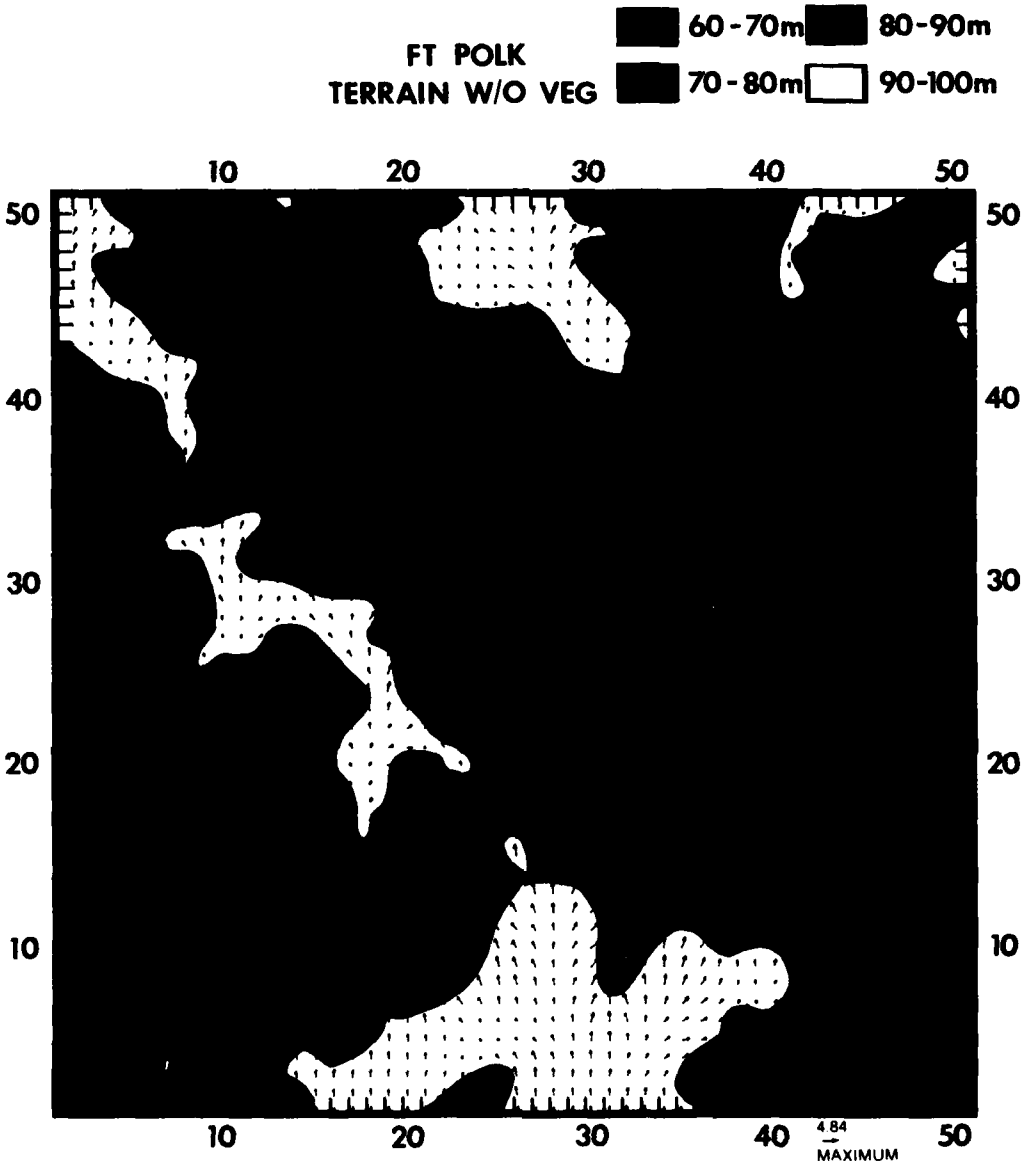

Figure 11a. Model Windfield for Experiment 1a Showing Wind Velocity Vectors for Cases With No Vegetation and Uniform Surface Roughness (Length Proportional to Speed; See Maximum Vector Displayed in Lower Right). Terrain elevations are highlighted as in Figure 2

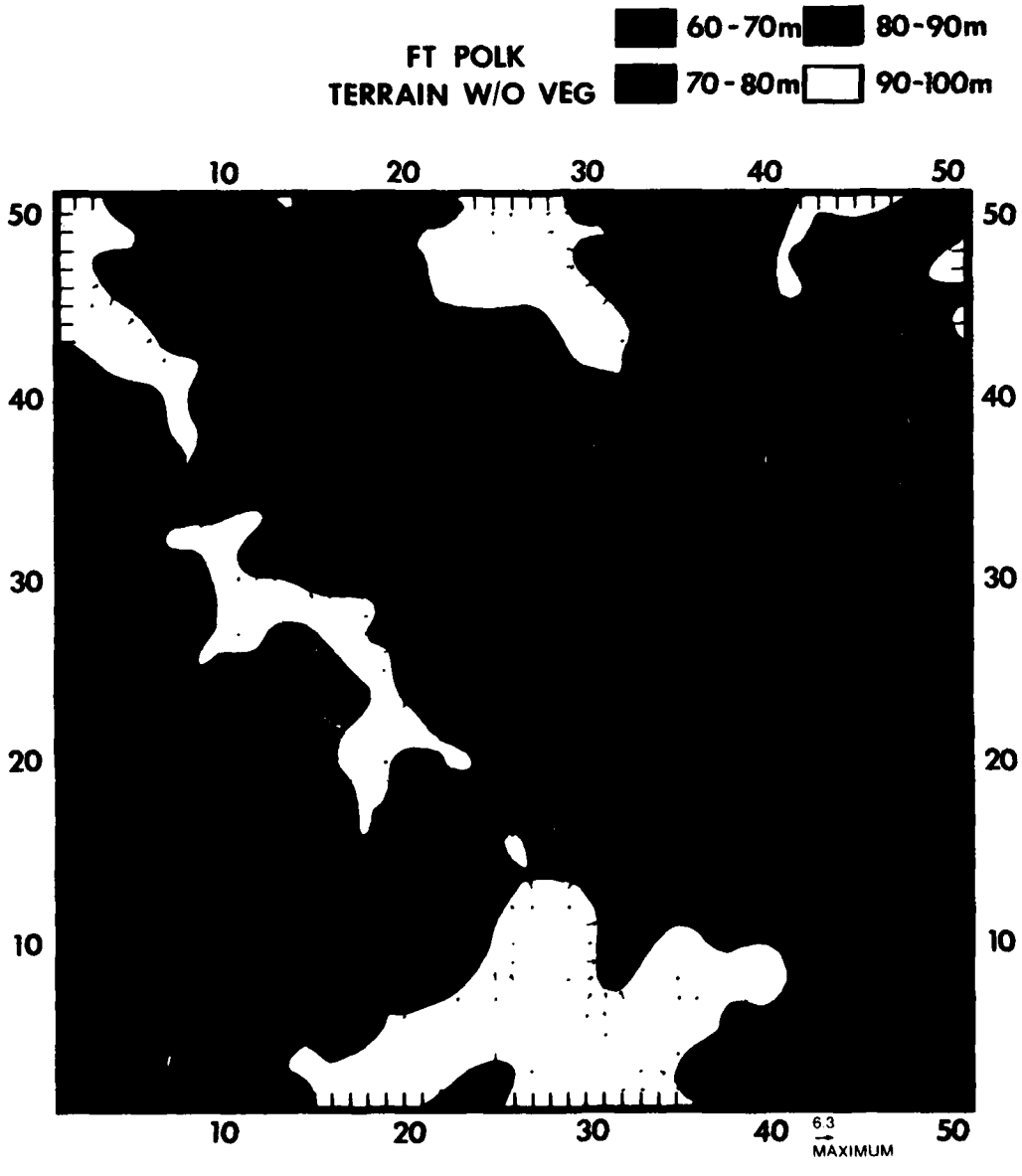

Figure 11b. Model Windfield for Experiment 7a Showing Wind Velocity Vectors for Cases With No Vegetation and Uniform Surface Roughness (Length Proportional to Speed; See Maximum Vector Displayed in Lower Right). Terrain elevations are highlighted as in Figure 2

from experiment 3a contains a well defined southeasterly component along the Six-mile Creek valley which did not appear in the experiment with vegetation (compare Figures 12a and 9a). The presence of nonhomogeneous vegetation in experiment 3 seems to disrupt the southeasterly flow along the valley, with the lowland marshes distorting it. The southeasterly flow in experiment 3a appears to be partially caused by the channeling effects of the parallel ridge and highlands in the northern and eastern areas of the domain. We do not believe this is a valley wind because a corresponding northwesterly mountain wind does not appear in the stable case.

When the magnitude of the stability is increased (experiment 4a), the southeasterly flow is maintained and the windfield remains essentially the same as in experiment 3a. Therefore, we do not show the windfield for this experiment. The appearance of the southeasterly flow along the valley in the experiments without vegetation would have important effects on transport and diffusion. The results suggest that, in the cases without vegetation, chemicals could be transported further up the valley than in the vegetation cases, where diffusion could take place in the localized lowland marshes. When initially calm winds are introduced (experiment 8a; Figure 12b), the localized upslope flows appear over different areas than they do in the vegetation case (experiment 8; Figure 9c). When an initial wind speed of $10\ ms^{-1}$ is introduced (experiment 5a; Figure 12c), the windfield is nearly uniform, more uniform, in fact, than in the vegetation case (experiment 5; Figure 9d). This probably occurs because the terrain is more uniform without the vegetation.

3.3.6 NEUTRAL CONDITIONS WITHOUT VEGETATION

A curious result comes from this experiment (experiment 6a; Figure 13). The windfield for this case is totally uniform, remaining unchanged from initial conditions. The effect of terrain uniformity on the flow was discussed at the end of Section 3.3.5. To determine if the uniform windfield was the result more of terrain and stability conditions than of initial wind speeds, experiments were run with neutral conditions and an initial wind of $2\ ms^{-1}$ (no vegetation), and other experiments were run with no terrain and uniform roughness for differing windspeeds. The results of these experiments led us to conclude that the removal of the vegetation and imposition of neutral conditions was responsible for the uniform windfield in experiment 6a.

4. CONCLUSIONS

The first phase of the ASL windflow model evaluation has been completed. We have shown that the model, despite the simple physics involved, is quite ver-

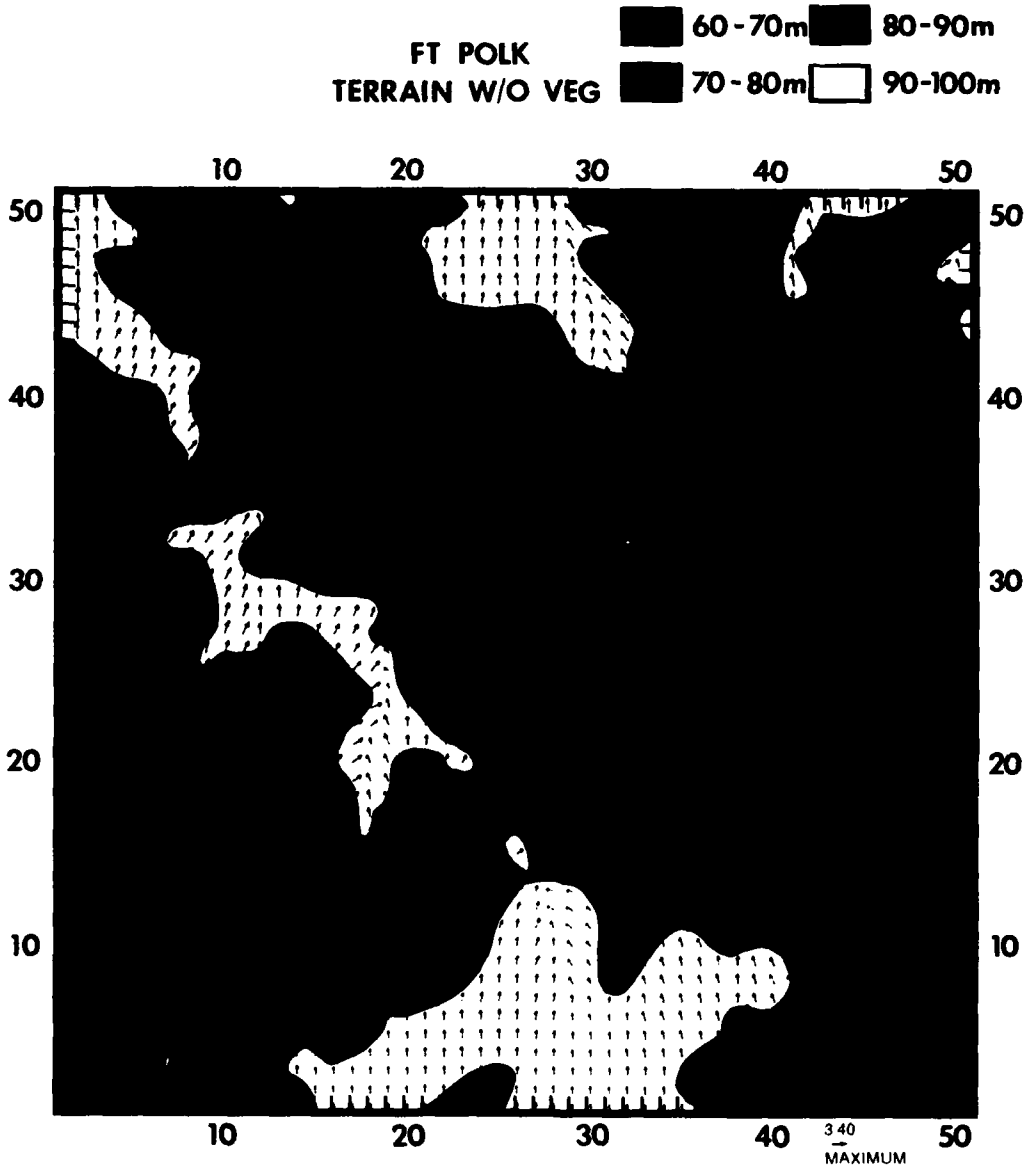

Figure 12a. Model Windfield for Experiment 3a Showing Wind Velocity Vectors for Cases With No Vegetation and Uniform Surface Roughness (Length Proportional to Speed; See Maximum Vector Displayed in Lower Right). Terrain elevations are highlighted as in Figure 2

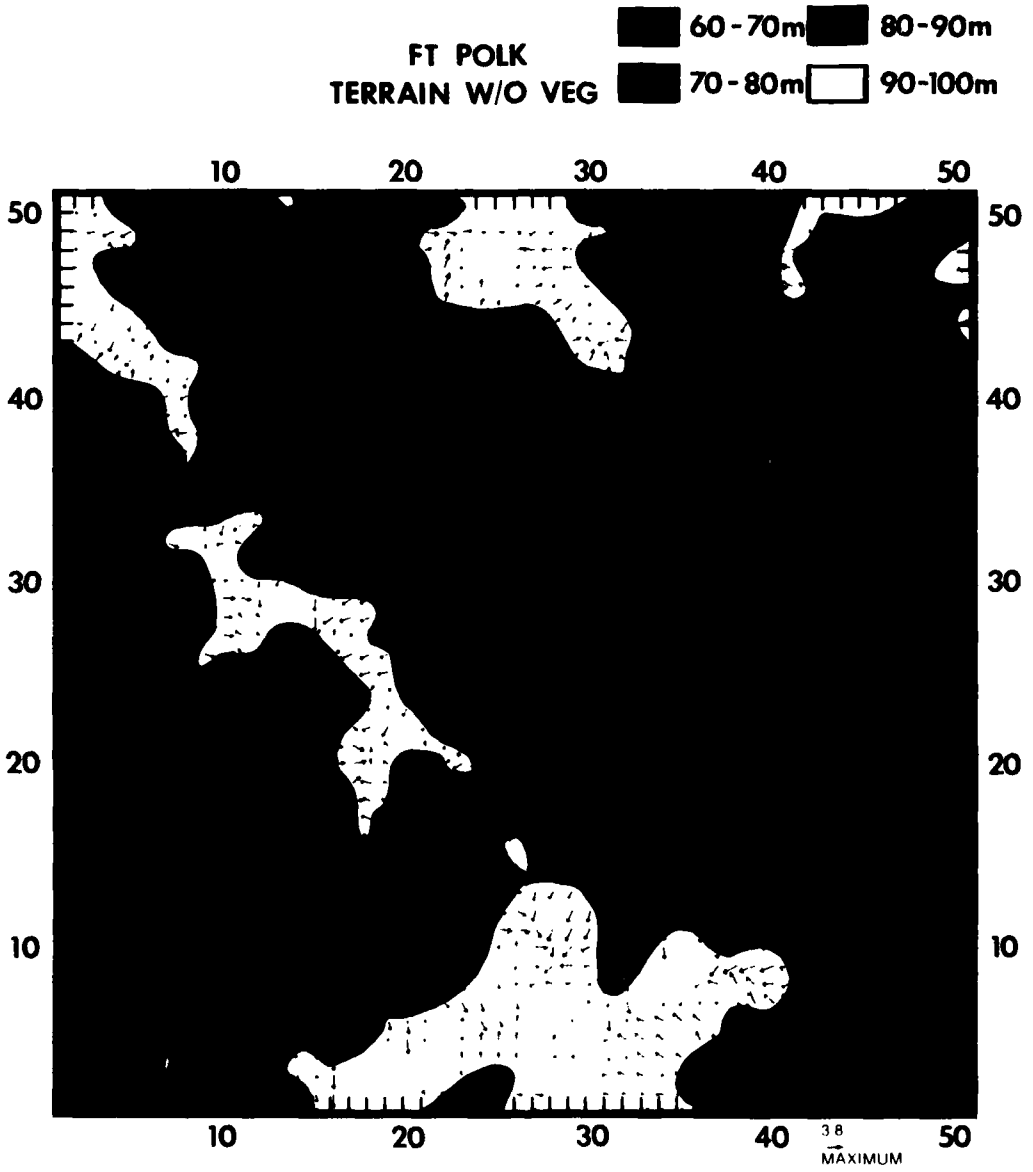

Figure 12b. Model Windfield for Experiment 8a Showing Wind Velocity Vectors for Cases With No Vegetation and Uniform Surface Roughness (Length Proportional to Speed; See Maximum Vector Displayed in Lower Right). Terrain elevations are highlighted as in Figure 2

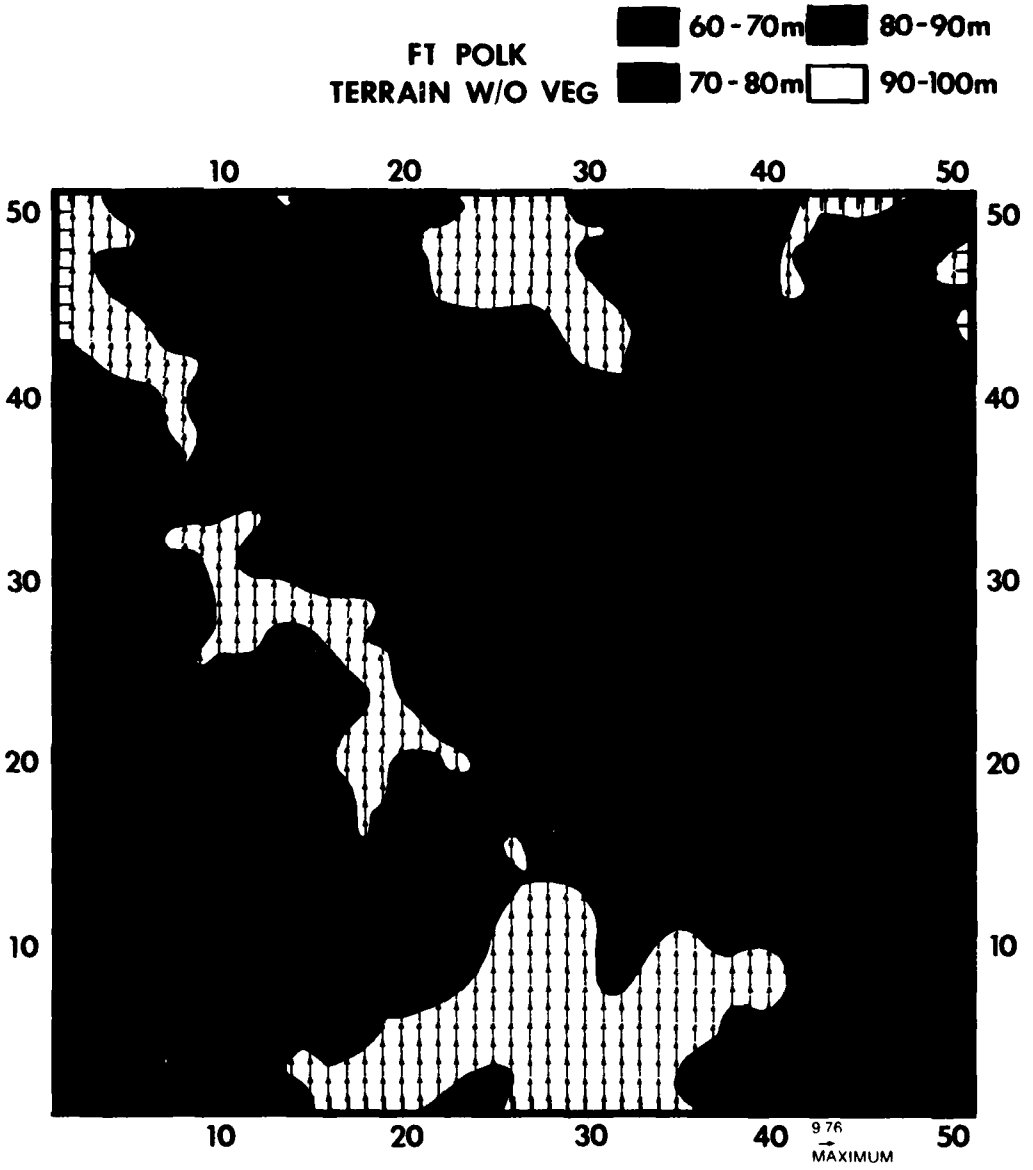

Figure 12c. Model Windfield for Experiment 5a Showing Wind Velocity Vectors for Cases With No Vegetation and Uniform Surface Roughness (Length Proportional to Speed; See Maximum Vector Displayed in Lower Right). Terrain elevations are highlighted as in Figure 2

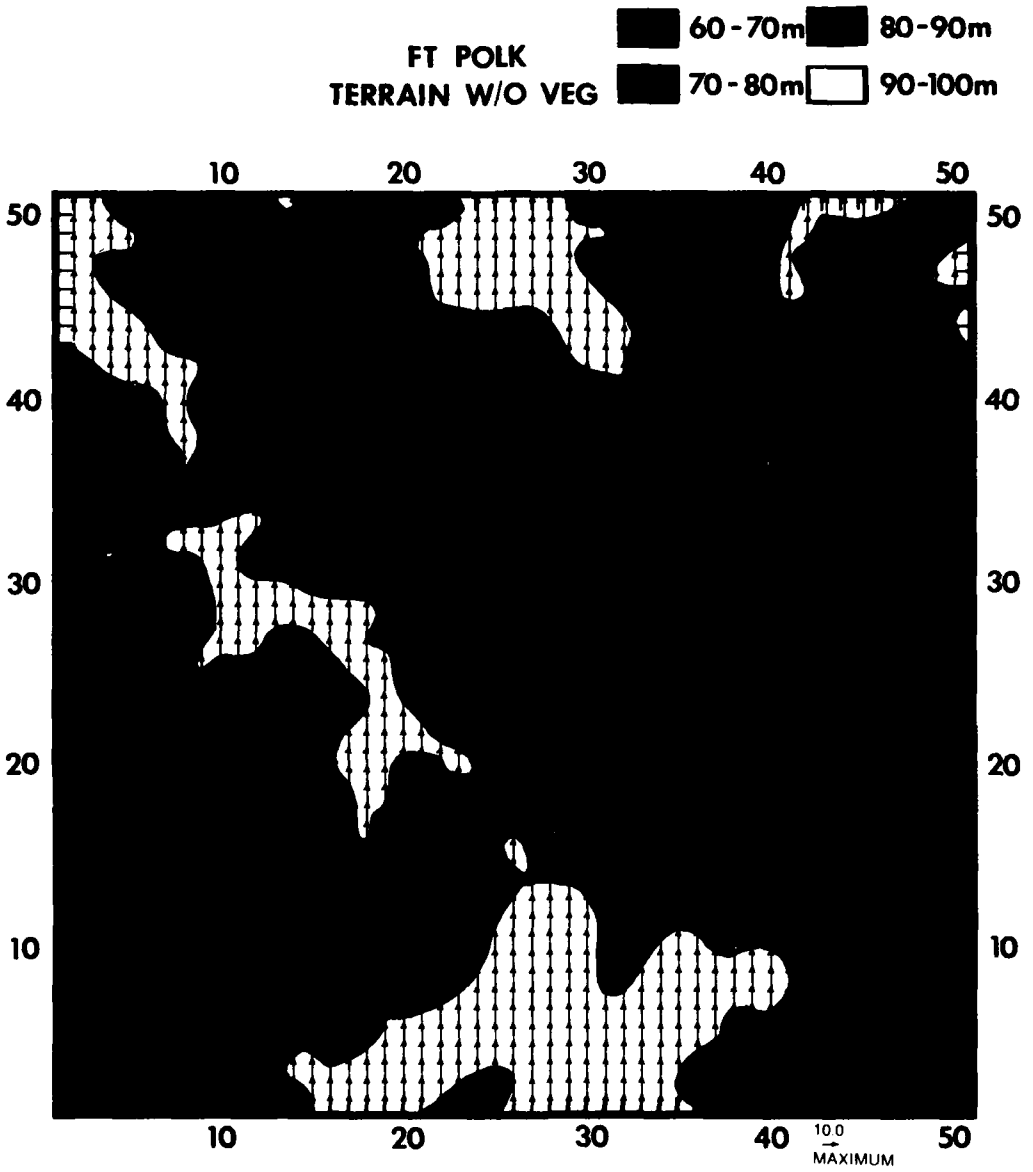

Figure 13. Model Windfield Showing Wind Velocity Vectors for Neutral Conditions With No Vegetation and Uniform Surface Roughness (Length Proportional to Speed; See Maximum Vector Displayed in Lower Right). Terrain elevations are highlighted as in Figure 2

satile and capable of simulating different types of flows under varying topographic and stability conditions. This section summarizes the modeling results, discusses some of the limitations of the windflow model, and describes the future research with the model that will be done at AFGL.

4.1 Summary of Results

The ASL windflow model can simulate stability-influenced, topographically driven flows, such as nocturnal drainage and upslope flow. The model can simulate these flows under light wind or calm conditions, and it produces fairly uniform windfields under high wind conditions. Under neutral conditions, the model produces essentially uniform windfields. The model shows a tendency towards intensifying the slope winds as the magnitude of the buoyancy is increased, while weakening the winds elsewhere.

Examination of the total kinetic energy (KE) over the domain for different stability conditions revealed several insights consistent with the model physics. The KE is sensitive to the magnitude of the buoyancy, increasing faster for cases with larger buoyancy magnitudes. However, this result only appears for cases with light wind conditions. Under high wind conditions, the KE decreases through the model integration. Under neutral conditions, the model KE decreases during the model integrations, regardless of the initial wind conditions. These results are consistent with the adjustment taking place through the integral of Eq. (1), and are thus dependent upon the buoyancy, initial wind speed, and topography in the model. The strongest winds generally appear over areas with the greatest terrain gradients.

The results of the model experiments also illustrate the importance of including the effects of vegetation as they relate to the modification of terrain geometry. The addition of vegetation in the model alters the topographically induced flows, creating localized convergence zones in low-lying marshes under drainage (stable) conditions, and disrupting the southeasterly channeled flow along the Sixmile Creek valley in the unstable cases. The changes in the flow patterns by addition of vegetation are consistent with the model physics, since the vegetation alters the terrain slopes. It was determined that variable surface roughness is a second-order effect in the model, and that the changes in the flow patterns are caused primarily by the presence of vegetation as used to modify the terrain geometry.

4.2 Limitations of the Research

The goal of this work is to produce an operational prediction system for toxic chemical transport and diffusion. The numerical model described in this report seems well suited for adaptation to an operational system, but it has some impor-

tant limitations which should be pointed out.

The simple physics of the model as described by Eq. (1) leaves out some important terms, such as surface-layer momentum fluxes. Even though these fluxes can be assumed to be nearly constant in the surface layer, there is no coupling of the surface layer to the mixed layer aloft. This is an important weakness in the unstable cases, where increasing the instability should lead to a stronger mixing and more uniform wind flow, but this does not appear in the model.

The vertical dimension is only considered in the power law formulation using the Businger et al[27] wind profiles. In the case of Fort Polk, it can be assumed that the buoyancy field is fairly uniform, but, over steeper terrain slopes, effects of differential surface heating become more important. In the latter case, a thermodynamic equation or a surface energy budget might have to be added to consider the effects of differential surface heating and vertical mixing of heat, momentum, and moisture on the surface layer.

Another useful addition to the model would be the effects of the vegetation canopy itself on the wind profiles and stability of the surface layer. Modifications to the ASL model to include vegetation canopy effects are presently being made at ASL.*

Obvious limitations exist on the availability of meteorological observations on a scale such as the one we are using in this model. This problem is related both to the availability of input observations and to the verification of the model windfields. The model experiments conducted in this evaluation were not verified by observations over the Fort Polk area. Some data were collected over the Fort Polk region during a field experiment conducted in 1980,[19] but these were not adequate to use in a model verification study. However, the results presented here are reasonable approximations of the types of flows one would expect over complex terrain under varying stability conditions.

The fact that the terrain only varies by several 10s of m over Fort Polk does not mean that topographic flows cannot exist. Observational studies by Caughey et al[33] and Lenschow et al,[34] and modeling studies by Brost and Wyngaard[35] show that cold air drainage and slope flows can occur with terrain slopes as small as 0.0014.[33] These flows were also shown to have significant effects on the structure of the stable boundary layer. The fact that the presence of tall vegetation can alter

---

*Cionco, R.M. Personal communication.

33. Caughey, S.J., Wyngaard, J.C., and Kaimal, J.C. (1979) Turbulence in the evolving stable boundary layer, J. Atmos. Sci. 36:1041-1052.

34. Lenschow, D.H., Stankov, B.B., and Mahrt, L. (1979) The rapid morning boundary-layer transition, J. Atmos. Sci. 36:2108-2124.

35. Brost, R.A., and Wyngaard, J.C. (1978) A model study of the stably stratified planetary boundary layer, J. Atmos. Sci. 35:1427-1440.

the terrain slope is also consistent with the vegetation/no vegetation results presented in this study. The model results concerning the effects of vegetation on the flow are consistent with those documented by Geiger[36] and others. Thus, the next step in the model evaluation would be to verify the windfields against actual field observations.

4.3 Future Research With the Model at AFGL

With the first phase of the model evaluation complete, the attention at AFGL will now shift to verification of the model windfields against observations. Future work calls for running the ASL model using simulated and actual meteorological data over Vandenberg AFB, Calif. Again, detailed terrain information (50-m grid spacings on the terrain data tape) is available. The model domain will be chosen to cover an area the size of the southern launch complex, where meteorological tower data are available for use as multiple input observations and for verification. The simulated data studies will use the same format as the Fort Polk study (climatological soundings) in order to study the sensitivity of the model to stability and the steep terrain slopes that appear over the Vandenberg area. The tower data experiments will likely make use of the archived data base available for this area.[37]

The proposed work intends to study various meteorological situations of interest, as well as the model's sensitivity to the number and spatial distribution of input observations used. The results of the proposed work will, we hope, yield results quantifying the real-time input data requirements for the model and reveal detailed information about the surface-layer windflow over the area from which the Space Transportation System (STS) will be launched in the future.

---

36. Geiger, R. (1965) The Climate Near the Ground, Harvard University Press, Cambridge, Mass. p. 356.

37. Schacher, G.E., and Stanton, T.P. (1984) Mean Flow and Turbulence in Complex Terrain NPS/Vandenberg Measurement System, NPS-61-84-005, Naval Postgraduate School, Monterey, Calif.

References

1. Fleischer, M.T. (1980) SPILLS - An Evaporation/Air Dispersion Model for Chemical Spills on Land, Shell Development Company, Westhollow Research Center, Houston, Tex.
2. Kunkel, B.A. (1983) Comparison of Evaporative Source Strength Models for Toxic Chemical Spills, AFGL-TR-83-0307, AD A139431.
3. Kunkel, B.A. (1984) An Evaluation of the Ocean Breeze/Dry Gulch Dispersion Model, AFGL-TR-84-0313, AD A157165.
4. Ball, J.A., and Johnson, S.A. (1978) Physically Based High Resolution Surface Wind and Temperature Analysis for EPAMS, ASL-CR-78-0043-1, U.S. Army Atmospheric Sciences Laboratory, White Sands Missile Range, N. Mex.
5. Holdeman, J.T. (1982) Modeling the tropospheric wind field over complex terrain, Symposium on the Composition of the Non Urban Troposphere, Williamsburg, Va.
6. Dickerson, M.H. (1978) MASCON - A mass-consistent atmospheric flux model for regions with complex terrain, J. Appl. Meteorol. 17:241-253.
7. Dempsey, D.P., and Mass, C.F. (1983) A one-level mesoscale model for complex terrain, Proc. Sixth Conf. on Numerical Weather Prediction, Am. Meteorol. Soc., Boston, Mass. 343-347.
8. Haltiner, G.J. (1971) Numerical Weather Prediction, Wiley, New York.
9. Walmsley, J.L. (1983) Modeling of Boundary-Layer Wind Flow Above Complex Terrain: A Review, Report ARQB-83-005-L, Atmospheric Environment Service, Downsview, Ontario.
10. Lavoie, R.L. (1972) A mesoscale model of lake-effect storms, J. Atmos. Sci. 29:1025-1040.
11. Lavoie, R.L. (1974) A numerical model of trade wind weather on Oahu, Mon. Wea. Rev. 102:630-637.

12. Fox, D.G., Fosberg, M.A., Marlatt, W.E., and Reeser, W. (1976) Analysis of mountain air quality, Proc. Third Symposium on Atmospheric Turbulence, Diffusion, and Air Quality, Am. Meteorol. Soc., Boston, Mass. 470-475.

13. Ohmstede, W.D. (1981) The parameterization of battlefield dispersion-new frontiers, Workshop on the Parameterization of Mixed-Layer Diffusion, Las Cruces, N. Mex. 279-287.

14. Ohmstede, W.D., and Stenmark, E.B. (1981) A model for characterizing transport and diffusion of air pollution in the battlefield environment, Workshop on the Parameterization of Mixed-Layer Diffusion, Las Cruces, N. Mex. 416-423.

15. Cionco, R.M. (1981) A meteorological approach to chemical defense over complex terrain with vegetation, Workshop on the Parameterization of Mixed-Layer Diffusion, Las Cruces, N. Mex. 323-328.

16. Amlicke, B.B., and Coleman, I.W. (1984) High Resolution Wind (HRW) Model, MRC/WDC-R-089, Mission Research Corporation, Alexandria, Va.

17. Lanczos, C. (1970) The Variational Principles of Mechanics (4th ed), U. of Toronto Press, Toronto, pp. 106-110.

18. Dutton, J.A. (1976) The Ceaseless Wind, McGraw-Hill, New York, pp. 435-439.

19. Sadeh, W.Z., Law, F.W., Marlatt, W.E., Fox, D.G., Dietrich, D.L., and Cionco, R.M. (1982) A Survey of Micrometeorological Parameters Within a Forest Canopy at Fort Polk, Louisiana, ASL-CR-0100-1, U.S. Army Atmospheric Sciences Laboratory, White Sands Missile Range, N. Mex.

20. Bradshaw, P. (1969) The analogy between streamline curvature and buoyancy in turbulent shear flow, J. Fluid Mech. 36, Part 1:177-191.

21. Atkinson, B.W. (1981) Mesoscale Atmospheric Circulations, Academic Press, London, pp. 13-20.

22. Panofsky, H.A., and Dutton, J.A. (1984) Atmospheric Turbulence: Models and Methods for Engineering Applications, Wiley, New York, pp. 124-125.

23. Monteith, J.L. (1973) Principles of Environmental Physics, Edward Arnold Ltd., London, pp. 88-90.

24. Sellers, W.D. (1965) Physical Climatology, U. of Chicago Press, Chicago pp. 150-151

25. Lettau, H. (1969) Note on aerodynamic roughness-parameter estimation on the bases of roughness-element description, J. Appl. Meteorol. 8:828-832.

26. Tanner, C.B., and Pelton, W.L. (1960) Potential evapotranspiration estimates by the approximate energy balance method of Penman, J. Geophys. Res. 65:3391-3413.

27. Businger, J.A., Wyngaard, J.C., Izumi, Y., and Bradley, E.F. (1971) Flux-profile relationships in the atmospheric boundary layer, J. Atmos. Sci. 28:181-189.

28. McNider, R.T., and Pielke, R.A. (1984) Numerical simulation of slope and mountain flows, J. Climate and Appl. Meteorol. 23:1441-1453.

29. McNider, R.T. (1982) A note on velocity fluctuations in drainage flows, J. Atmos. Sci. 39:1658-1660.

30. Banta, R.M. (1982) An Observational and Numerical Study of Mountain Boundary-Layer Flow, Ph.D. thesis, Colorado State U., Ft. Collins, Colo.

31. Banta, R.M. (1984) Daytime boundary-layer evolution over mountainous terrain. Part I: Observations of the dry circulations, Mon. Wea. Rev. 112:340-356.

32. Orgill, M.M. (1981) Atmospheric Studies in Complex Terrain: A Planning Guide for Future Studies, PNL-3656, ASCOT/80/4, Pacific Northwest Laboratory, Richland, Wash.

33. Caughey, S.J., Wyngaard, J.C., and Kaimal, J.C. (1979) Turbulence in the evolving stable boundary layer, J. Atmos. Sci. 36:1041-1052.

34. Lenschow, D.H., Stankov, B.B., and Mahrt, L. (1979) The rapid morning boundary-layer transition, J. Atmos. Sci. 36:2108-2124.

35. Brost, R.A., and Wyngaard, J.C. (1978) A model study of the stably stratified planetary boundary layer, J. Atmos. Sci. 35:1427-1440.

36. Geiger, R. (1965) The Climate Near the Ground, Harvard University Press, Cambridge, Mass. p. 356.

37. Schacher, G.E., and Stanton, T.P. (1984) Mean Flow and Turbulence in Complex Terrain NPS/Vandenberg Measurement System, NPS-61-84-005, Naval Postgraduate School, Monterey, Calif.

END

DTIC

7-86